Ma, Q. & Yan, S. (2009). QALE-FEM for numerical modelling of non-linear interaction between 3D moored floating bodies and steep waves. INTERNATIONAL JOURNAL FOR NUMERICAL METHODS IN ENGINEERING, 78(6), pp. 713-756. doi: 10.1002/nme.2505

QALE-FEM for Numerical Modelling of Nonlinear Interaction between 3D Moored Floating Bodies and Steep Waves

Q.W. Ma*, S. Yan

School of Engineering and Mathematical Sciences

City University, London, EC1V 0HB, UK

Abstract

This paper presents further development of the QALE-FEM (Quasi Arbitrary Lagrangian-Eulerian Finite Element Method) based on a fully nonlinear potential theory to numerically simulate nonlinear responses of 3D moored floating bodies to steep waves. In the QALE-FEM (recently developed by the authors and applied to 2D floating bodies), the complex unstructured mesh is generated only once at the beginning of calculation and is moved to conform to the motion of boundaries at other time steps by using a robust spring analogy method specially suggested for this kind of problems, avoiding the necessity of high cost remeshing. In order to tackle challenges associated with 3D floating bodies, several new numerical techniques are developed in this paper. These include the technique for moving the mesh near body surfaces, the scheme for calculating velocity on 3D body surfaces and the ISITIMFB-M (Iterative Semi-Implicit Time Integration Method for Floating Bodies - Modified) procedure that is more efficient for dealing with the full coupling between waves and bodies. Using the newly developed techniques and methods, various cases for 3D floating bodies with motions of up to 6 degrees of freedom (DoFs) are simulated. These include a SPAR platform, a barge-type floating body and one or two Wigley Hulls in head seas or in oblique waves. For some selected cases, the numerical results are compared with experimental data available in the public domain and satisfactory agreements are achieved. Many results presented in this paper have not been found elsewhere to the best knowledge of the authors.

Keywords: QALE-FEM; Nonlinear water waves; Spring analogy method; Iterative procedure; 3D floating bodies; freely responses to waves with 6 degrees of freedom (DoFs).

* Corresponding author. Tel.: +44 20 7040 8159; fax: +44 20 7040 8566
E-mail address: q.ma@city.ac.uk (Q.W. Ma)

1. Introduction

To make use of resources in oceans, various moored structures, such as SPAR platforms, FPSOs (Floating Production Storage and Offloading vessels), floating breakwaters and floating storage systems, have been built and utilised. There is no doubt that more structures will be built and utilised in a foreseeable period of time, though their types or uses may be different. No matter what type they are and what purpose they are used for, one thing is in common, i.e., they are all under actions of waves. Sometimes these actions are very violent. In order to produce offshore structures that are safe, functional and economical, one must have a good understanding of interaction between structures and environmental waves. For this purpose, linear, second order or other simplified theories with different degrees of approximation (such as, strip theory, a theory based on fully nonlinear conditions on the free surface but linear conditions on body surfaces or linear conditions on the free surface but fully nonlinear conditions on bodies) have been well developed. They are often sufficient for routine design, in which one assumes that the motions of waves and/or structures are moderate. Reviews on the work associated with the simplified theories can be found in many publications (e.g., Beck & Reed [1] and Eatock Taylor [2]), which will not be given here. In many situations, however, one must consider extremely large steep waves and/or behaviours of bodies subjected to them. In such cases, fully nonlinear theory has to be adopted. Necessity of using fully nonlinear theory has been justified by many researchers, e.g. Liu, Xue & Yue [3] and Beck & Reed [1]. Models based on fully nonlinear theory can be divided into two groups. The first group solves the Navier-Stokes (NS) equations together with the continuity equation and proper boundary conditions while the second group deals with the Laplace equation with fully nonlinear boundary conditions. For brevity, the first group will be called NS Model and the second called FNPT (representing fully nonlinear potential theory) Model as in our previous papers, e.g. Yan & Ma [18]. Generally speaking, solving the equations for the NS Model is always a time consuming task and is much more difficult, particularly when floating bodies with motions of 6 degrees of freedom (DoFs) are included. As a result, the FNPT Model has been explored in many publications, which needs much less computational resources than the NS Model. In this model, of course, viscosity could not be precisely considered, though some empirical viscosity in motion equations of bodies may be introduced. Comparison with experimental data (e.g., [4] and [5]) has shown that the results obtained by using this model are accurate enough in many cases, in which breaking waves do not occur and/or structures involved are large. Therefore, the FNPT Model, instead of the NS Model, should be preferred if a case considered falls in this

category. However, it does not mean that solving the problems based on the FNPT Model is easy. Actually it is still very difficult, mainly due to the continuously moving of free surface and/or floating bodies and to the fact that their positions and attitudes are unknown prior to solution being found. In this work, the FNPT Model is adopted. On this basis, the review on the work using the NS Model will not be given here. Readers may be referred to, e.g., Beck and Read [1], Yang, Lohner & Lu [6], Idelsohn, Oñate, Del Pin & Calvo [7] and others therein.

(Table 1. Summary of problems about fully nonlinear interaction between waves and bodies)

In the context of fully nonlinear simulation based on the potential theory, bodies may or may not be included. For the problems without bodies, people are mainly interested in the wave dynamics. Review on this kind of problem will be presented in another paper (Yan & Ma [34]). Here, our attention will be concentrated on the fully nonlinear interaction between floating bodies and steep waves. In this framework, various problems may be summarized in Table 1. In this table, the problems are first grouped into these with fixed bodies (i.e., diffraction), these with bodies subjected to forced (prescribed) motions (i.e., radiation) and these with bodies freely responding to excitation of waves, which are listed in different columns from the left to the right. Compared with the problems about fixed bodies, these (about forced motions) to their immediate right are more difficult. That is mainly because the meshes near the body and free surfaces as well as their intersecting line (waterline) are required to be finer relative to those in other areas and are not easy to maintain such distribution, no matter which numerical method is used. For example, when a body is subjected to a large surge (or sway) motion, the finer mesh areas must follow the motion in the horizontal

direction to give good results. This clearly needs special attention. The problems about floating bodies freely responding to waves are even more difficult. The difference between freely floating bodies and those being fixed or subjected to forced motions is that for the former the coupling between the motions of waves and bodies has to be dealt with, which is not necessary for the latter. This feature leads to many challenging issues. The important one is that the position and velocity of body surfaces are unknown and have to be found simultaneously together with water waves by solving different dynamic equations. The second but not less important issue is to maintain the good mesh near bodies, which is a tougher task than in the situation of forced motions since one does not know where the bodies go prior to the solution being found. In addition, the stability is often of concern when body motions are fully coupled with water waves. A numerical procedure for the problems about bodies being fixed or subjected to forced motions may be stable but it is not necessarily stable for these with free responses by using the same time steps. One of examples was discussed by Koo & Kim [17]. Within the group of the problems about freely floating bodies, these with motions of 6 DoFs are more complicated than those with motions of 3 DoFs. That is not only because the case with 6 DoFs needs more computer resources and CPU time but also because some special issues demand more sophisticated numerical techniques. For example, in a head sea, in which a moored ship may undergo only 3-DoF motions, the sharp bow edge of the ship may not cause any numerical difficulty. However, if it is in an oblique wave, in which a moored ship must undergo 6-DoFs motions, this edge may cause the simulation to fail if no special treatment is applied. Compared to others, the problems involving freely-floating multi-bodies are obviously the most difficult.

Secondly, all the problems are grouped into 2D (two-dimensional) and 3D (three-dimensional) ones in Table 1. The 2D problems are relatively easier and may provide a good approximation in some cases. However, they could not generally represent the real problems in most cases, which are always three-dimensional in nature.

As can be seen in the table, a lot of publications have been devoted to solving the problems about the 2D and 3D fixed bodies and bodies with forced motions. A considerable number of publications are also devoted to 2D bodies freely responding to waves. However, the results on the 3D bodies freely responding to waves are still very limited even for simpler cases with 3 DoFs. The works on 3D bodies with 6-DoFs free responses are hardly found at present in the public domain. It is stressed again that the references given in Table 1 are only these dealing with fully-nonlinear interaction between bodies and waves by using the

fully nonlinear potential theory and thus do not include those using various simplified theories. Even in this context, the references in the table may not be considered as complete, though most typical developments are believed to be included.

The problems formulated by the FNPT Model are usually solved by a time marching procedure suggested by Longuet-Higgins & Cokelet [35] and used by many others (such as Vinje & Brevig [36]; Lin, Newman & Yue [37]; Wang, Yao & Tulin [38]; Grilli, Guyenne & Dias [39]). In this procedure, the key task is to solve boundary value problems (BVPs) by using a numerical method, such as a boundary element (panel) or boundary integral method (BEM) and a finite element method (FEM). The conventional BEM (linear or higher order) has been attempted by many researchers (e.g., Kashiwagi [15, 40]; Ferrant [20]; Liu, Xue & Yue[3]; Corte and Grilli[26]). An alternative one called desingularized boundary integral method was employed by Cao, Schultz & Beck [41], Cao, Beck & Schultz [13], Celebi, Kim & Beck [30] and Kim, Celebi & Kim [31], Celebi [25] and so on. Recently, Bai and Eatock Taylor [28, 32] combined the BEM with domain decomposition technique (extending the idea of Wang, Yao & Tulin [38] to 3D cases) to study the diffraction and radiation of cylinders. It is noted that a fast BEM method was recently published by Fochesato & Dias [42], which could be 6 times faster than the conventional BEM as shown by their numerical tests on 3D overturning waves, but it has not yet been found to be applied to wave-body interactions, though it has such potential. The FEM was developed by Wu & Eatock Taylor [43, 44], Westhuis & Andonowati [45] and Clauss & Steinhagen [4] for 2D cases and by Ma, Wu & Eatock Taylor [23, 24] and Ma [21] for 3D cases. Wu and Eatock Taylor [16] have suggested a method combining the BEM with FEM and applied it to 2D problems about free responses of a submerged cylinder, in which the BEM is used in a small region surrounding a body while the outer region is modelled by a simple structured mesh of finite elements.

Both the BEM and the FEM have been proved efficient but the later requires less memory and therefore may be computationally more efficient for fully nonlinear wave-body problems, as indicated by Ma, Wu & Eatock Taylor [23] and Wu & Eatock Taylor [43]. A disadvantage of the FEM, however, is that a complex unstructured mesh, which is necessary for complicated geometries to achieve accurate results, may need to be regenerated at every time step to follow the motions of waves and bodies. Repeatedly regenerating such a mesh may take a major part of CPU time and so makes the overall simulation very slow. In order to reduce the CPU time spent on meshing, simple structured meshes have been used by Ma, Wu & Eatock Taylor [23,

24], Wu & Eatock Taylor [43, 44] and Ma [21]. These were improved by Wu and Hu [46], Wang & Wu [10] and Wang, Wu & Drake [27], in which the unstructured meshes are generated only on the free surface while the mesh below it are obtained by drawing lines or curves from each node on the free surface, depending on the shape of the body. Turnbull, Borthwick & Eatock Taylor [8] and Heinze [9] adopted a hybrid structured-unstructured mesh for 2D problems, which is unstructured near a body and structured in the outer region. However, these techniques are either still time-consuming or restricted to the cases for bodies with special shapes and/or undergoing only translational motions. The problem with meshing has become a bottleneck in the development of more efficient methods dealing with the interaction between water waves and freely floating bodies by using the FEM. To overcome the difficulty, Ma and Yan [47] have invented a new method called QALE-FEM (Quasi Arbitrary Lagrangian-Eulerian Finite Element Method). The main idea of this method is that the complex unstructured mesh is generated only once at the beginning of calculation and is moved at other time steps to conform to motions of boundaries by using a robust method. This allows one to use an unstructured mesh with any degree of complexity without the need of regenerating it at every time step and to model complex motions of 6 DoFs. Its promising features have been shown by simulating various 2D problems in Yan & Ma [18, 19]. In the cited papers by the authors, the QALE-FEM was compared with conventional FEM in terms of computational efficiency and accuracy for various 2D cases. It was concluded that the QALE-FEM required less than 15% of the CPU time demanded by the conventional FEM at the same accuracy level. In Yan and Ma [34], the efficiency of the method is further compared with the fast BEM by Fochesato & Dias [42]. Both the methods are applied to simulate 3D overturning waves with the same level of accuracy, which last for the same duration and propagate in the same domain. The comparison showed that the QALE-FEM can be at least 10 times faster.

To deal with full coupling between waves and freely-responding bodies, one needs to evaluate the time derivative of velocity potential. This may be achieved by applying a direct finite difference scheme but it has been proved to be unstable by many researchers. The better way is to solve a boundary value problem (BVP) about the term. However this BVP depends on the body velocity that is unknown at the current step prior to finding the time derivative of velocity potential. To overcome this difficulty, four types of approach have been suggested by other researchers for different numerical methods. These are the iterative procedure (Cao, Beck & Schultz [13]), Dalen & Tanizawa's method (Dalen [12], Tanizawa [48]), the mode-decomposition method (Vinje & Brevig [36]) and the indirect method (Wu & Eatock Taylor [11]). Using one of these

methods and the BEM, Tanizawa [49], Tanizawa & Minami [50] and Tanizawa, Minami & Naito [51] simulated 2D barge-type freely-floating body, followed by Koo & Kim [17]. Kashiwagi, Momoda & Inada [52], Kashiwagi [15] and Contento [14] investigated the wave-induced motions of 2D floating bodies with more complicated shapes. Tanizawa [53] and Tanizawa & Minami [33] simulated the interaction between waves and 3D Wigley Hull with motions of 3 DoFs. In the community of researchers who employ the FEM, Wu and Eatock Taylor [16] applied the indirect method to model the problems about a 2D submerged cylinder. However, in all the papers, the body velocity is estimated explicitly. The explicit procedure may be satisfactory if time steps and so changes in the velocity and acceleration in one step are sufficiently small; otherwise, it may degrade the accuracy and even lead to instability. Yan & Ma [18] developed an iterative procedure called ISITIMFB (Iterative Semi-Implicit Time Integration Method for Floating Bodies) procedure that is based on the similar principle to that of Cao, Beck & Schultz [13] but is different from the later in that the body velocity and acceleration in the ISITIMFB procedure is estimated implicitly. This procedure has been demonstrated to be efficient and to be the best one matching the QALE-FEM by using the cases for 2D floating bodies.

As has been indicated, all the references cited above have presented results for 2D bodies or for 3D bodies only with motions of up to 3 DoFs, no matter what numerical methods and procedures were used. In this paper, the QALE-FEM is further developed to deal with the problems about 3D floating bodies with free responses of 6 DoFs, fully coupled with nonlinear water waves. In order to tackle challenges associated with 3D floating bodies, several new numerical techniques are developed. These mainly include the technique for moving mesh near body surfaces, the scheme for calculating fluid velocity on moving 3D body surfaces and the modified version of the iterative procedure - the ISITIMFB-M, which is more efficient for dealing with the full coupling between waves and bodies. Using the new developed techniques and methods, various cases associated with the nonlinear interaction between waves and different types of floating body, i.e., SPAR platforms, barge-type 3D floating bodies and Wigley Hulls, are simulated. Many results are not found to be published before to our best knowledge.

2. Mathematical model and FEM formulation

Similar to our previous papers ([18-19,47 and 55]), waves are generated by a piston-like wavemaker in a rectangle tank as shown in Fig. 1. The wavemaker is mounted at the left end and a damping zone with a

Sommerfeld condition (see [21, 23], for details) is applied at the right end of the tank in order to suppress the reflection. A Cartesian coordinate system is used with the *oxy* plane on the mean free surface and with the z-axis being positive upwards. A floating body is centred at x=0 initially and moored to the bed or walls of the tank unless mentioned otherwise. To describe the attitude of the floating body, a body-fixed coordinate system ($O_b x_b y_b z_b$) is employed, in which all axes go through the centre of gravity of the body with x_b-axis parallel to the keel and z_b-axis initially parallel to z-axis.

[Figure1]

Fig. 1. Sketch of fluid domain

2.1. FNPT Model for fluid

Similar to the usual formulation for the FNPT Model, the velocity potential (ϕ) satisfies Laplace's equation,

$$\nabla^2\phi = 0 \tag{1}$$

in fluid domain. On the free surface $z = \zeta(x, y, t)$, it satisfies the kinematic and dynamic conditions in the following Lagrangian form,

$$\frac{Dx}{Dt} = \frac{\partial\phi}{\partial x}, \frac{Dy}{Dt} = \frac{\partial\phi}{\partial y}, \frac{Dz}{Dt} = \frac{\partial\phi}{\partial z} \tag{2}$$

$$\frac{D\phi}{Dt} = -gz + \frac{1}{2}|\nabla\phi|^2 \tag{3}$$

where $\frac{D}{Dt}$ is the substantial (or total) time derivative following fluid particles and g is the gravitational acceleration. In Eq. (3), the atmospheric pressure has been taken as zero. On all rigid boundaries, such as the wavemaker and the floating body, the velocity potential satisfies

$$\frac{\partial\phi}{\partial n} = \vec{n}\cdot\vec{U}(t)\,, \tag{4}$$

where $\vec{U}(t)$ and $\vec{n}$ are the velocity and the outward unit normal vector of the rigid boundaries, respectively.

2.2. Motion equations of a floating body

The displacements, velocities and accelerations of a floating body are governed (see, e.g., [18, 21, 54]) by

$$[M]\dot{\vec{U}}_c = \vec{F}\,, \tag{5}$$

$$[I]\dot{\vec{\Omega}} + \vec{\Omega} \quad [I]\vec{\Omega} = \vec{N}\,, \tag{6}$$

$$\frac{d\vec{S}}{dt} = \vec{U}_c\,, \tag{7}$$

$$[B]\frac{d\vec{\theta}}{dt} = \vec{\Omega}\,, \tag{8}$$

where $\vec{F}$ and $\vec{N}$ are the external forces and moments acting on the floating body, $\vec{U}_c$ and $\dot{\vec{U}}_c$ the translational velocity and acceleration of its gravitational centre, $\vec{\Omega}$ and $\dot{\vec{\Omega}}$ its angular velocity and acceleration, $\vec{\theta}(\alpha,\beta,\gamma)$ the Euler angles and $\vec{S}$ the translational displacements. In Eq. (5) and (6), [*M*] and [*I*] are the mass and inertia-moment matrixes, respectively; and [*B*] in Eq. (8) is the transformation matrix formed by Euler angles and defined as,

$$[B] = \begin{bmatrix} \cos\beta\cos\gamma & \sin\gamma & 0 \\ -\cos\beta\sin\gamma & \cos\gamma & 0 \\ \sin\beta & 0 & 1 \end{bmatrix} \tag{9}$$

Once $\vec{U}_c$ and $\vec{\Omega}$ are known, the velocity at a point on the body surface is determined by

$$\vec{U} = \vec{U}_c + \vec{\Omega} \quad \vec{r}_b\,, \tag{10}$$

where $\vec{r}_b$ is the position vector of a point on the body surface relative to the gravitational centre.

2.3. Force and moment calculation

The external forces ($\vec{F}$) and moments ($\vec{N}$) acting on a body in Eqs. (5) and (6) can be evaluated by,

$$\vec{F} = -\rho \iint_{S_b} \left(\frac{\partial \phi}{\partial t} + \frac{1}{2}|\nabla\phi|^2 + gz \right) \vec{n} ds + \vec{f}_m\,, \tag{11}$$

$$\vec{N} = -\rho \iint_{S_b} \left(\frac{\partial \phi}{\partial t} + \frac{1}{2}|\nabla\phi|^2 + gz \right) \vec{r}_b \quad \vec{n} ds + \vec{N}_m\,, \tag{12}$$

where S_b denotes the wetted body surface, $\vec{f}_m$ and $\vec{N}_m$ are forces and moments due to mooring lines. Because this paper focuses on wave-body interaction, the mooring lines are approximated by using nonlinear springs, i.e.,

$$\vec{f}_m = k_m \vec{S}_m \tag{13}$$

$$\vec{N}_m = \vec{r}_m \quad \vec{f}_m \tag{14}$$

in which $\vec{S}_m$ is the displacement of a mooring point, k_m is the spring stiffness (possibly depending on $\vec{S}_m$) and $\vec{r}_m$ is the position vector of a mooring point relative to the gravitational centre of the floating body.

As can be seen, the time derivative of the velocity potential ($\partial\phi/\partial t$) is required and is critical for accurately calculating forces and moments. Although it may be estimated by using a time difference scheme, it is more stable to find the term by solving a BVP about it. The BVP about $\partial\phi/\partial t$ is defined by,

$$\nabla^2\left(\frac{\partial\phi}{\partial t}\right) = 0 \tag{15}$$

in the fluid domain. On the free surface $z = \zeta(x, y, t)$, it is estimated by

$$\frac{\partial\phi}{\partial t} = -g\zeta - \frac{1}{2}|\nabla\phi|^2 . \tag{16}$$

On all rigid boundaries, it satisfies

$$\frac{\partial}{\partial n}\left(\frac{\partial\phi}{\partial t}\right) = [\dot{\vec{U}}_c + \dot{\vec{\Omega}} \quad \vec{r}_b] \cdot \vec{n} - \vec{U}_c \cdot \frac{\partial\nabla\phi}{\partial n} + \vec{\Omega} \cdot \frac{\partial}{\partial\vec{n}}[\vec{r}_b \quad (\vec{U}_c - \nabla\phi)] . \tag{17}$$

As mentioned in §1 and evidenced in Eq. (17), there is a difficulty with solving Eqs. (15) to (17) together with Eqs. (1) to (12) if bodies freely respond to the excitation of waves. As can be seen from Eq. (17), the velocity and acceleration of the body must be known to solve the BVP about $\partial\phi/\partial t$. However, in the cases involving free-response floating bodies, they depend on the forces and moments in Eqs. (11) and (12) as shown in Eqs. (5) and (6). In turn, to find the forces and moments, one needs the term of $\partial\phi/\partial t$. The schemes to overcome this dilemma will be discussed in §3.4 below.

2.4. FEM formulation

The full details about the FEM formulation have been described in our previous publications (see, for example [23]). Only a summary is given herein. The problem described by Eqs. (1) to (4) is solved by using a time step marching procedure as mentioned before. At each time step, the free surface and the potential

values on it are known. Thus, the boundary condition for the potential on the free surface can be replaced by a Dirichlet condition:

$$\phi = f_p \,, \tag{18}$$

where f_p is the potential value on the free surface, which can be estimated by using Eq. (3) and a time integration scheme. Therefore, the unknown velocity potential in the fluid domain can be found by solving a mixed BVP which is defined by Eqs. (1), (4) and (18). To do so, the fluid domain is discretised into a set of small tetrahedral elements and the velocity potential is expressed in terms of a linear shape function, $N_J(x, y, z)$:

$$\phi = \sum_J \phi_J N_J(x, y, z) \,, \tag{19}$$

where ϕ_J is the velocity potential at Node J. Using the Galerkin method, the Laplace equation and the boundary conditions are discretised as follows,

$$\iiint_{\forall} \nabla N_I \cdot \sum_{\substack{J \\ J \notin S_P}} \phi_J \nabla N_J d\forall = \iint_{S_n} N_I f_n dS - \iiint_{\forall} \nabla N_I \cdot \sum_{\substack{J \\ J \in S_P}} (f_p)_J \nabla N_J d\forall \,, \tag{20}$$

where S_P represents the Dirichlet boundary, on which the velocity potential f_p is known, and S_n represents the Neumann boundary, on which the normal derivative of the velocity potential f_n is known. Eq. (20) can further be written in the matrix form:

$$[A]\{\phi\} = \{B\} \,, \tag{21a}$$

where

$$\{\phi\} = [\phi_1, \phi_2, \phi_3, \ldots, \phi_I, \ldots]^T \qquad (I \notin S_P) \,, \tag{21b}$$

$$A_{IJ} = \iiint_{\forall} \nabla N_I \cdot \nabla N_J d\forall \qquad (I \notin S_P, J \notin S_P), \text{ and} \tag{21c}$$

$$B_I = \iint_{S_n} N_I f_n dS - \iiint_{\forall} \nabla N_I \cdot \sum_{J \in S_P} (f_p)_J \nabla N_J d\forall \qquad (I \notin S_P). \tag{21d}$$

The algebraic Eq. (21) is solved by using a conjugate gradient iterative method with SSOR pre-conditioner and optimised parameters ([21]).

The problem about $\partial\phi/\partial t$ described in Eqs. (15) to (17) is solved also by using the above method with ϕ and the boundary conditions for it are replaced by $\partial\phi/\partial t$ and corresponding boundary conditions for $\partial\phi/\partial t$. Nevertheless, Eq. (17) is more complicated than its counterpart (Eq. 4) because the former contains the

second order derivative in the normal vector direction, which can degrade the numerical accuracy. To avoid this, that equation is equivalently changed to:

$$\frac{\partial}{\partial n}\left(\frac{\partial \phi}{\partial t}\right)=[\vec{U}_c+\dot{\vec{\Omega}}\quad \vec{r}_b-\vec{\Omega}\quad \vec{U}_c]\cdot\vec{n}-(\dot{\vec{\Omega}}\quad \vec{n})\cdot\nabla\phi-\frac{\partial\nabla\phi}{\partial n}\cdot(\vec{U}_c+\dot{\vec{\Omega}}\quad \vec{r}_b) \tag{22a}$$

with

$$\frac{\partial\nabla\phi}{\partial n}==-\left[\frac{\partial}{\partial\tau_1}\left(\frac{\partial\phi}{\partial\tau_1}\right)+\frac{\partial}{\partial\tau_2}\left(\frac{\partial\phi}{\partial\tau_2}\right)\right]\vec{n}+\frac{\partial}{\partial\tau_1}(\frac{\partial\phi}{\partial n})\vec{\tau}_1+\frac{\partial}{\partial\tau_2}(\frac{\partial\phi}{\partial n})\vec{\tau}_2\,, \tag{22b}$$

where $\vec{\tau}_1$ and $\vec{\tau}_2$ are two tangential unit vectors at the same point on the body surface as $\vec{n}$. More details about derivation and numerical implementation of these equations are given by Yan [55].

3. QALE-FEM for problems about 3D floating bodies

As mentioned in the Introduction, the QALE-FEM published in [18, 47] will be further developed in this paper to deal with more complicated problems about 3D floating bodies. This method includes three key elements in comparison with the conventional FEM method presented in [23]: (1) the scheme for moving mesh, (2) the method for estimating the velocity on the free surface and body surfaces and (3) the iterative procedure to deal with the full coupling between freely-responding floating bodies and water waves. All these elements have been described for 2D floating bodies in [18]. In this section, the three elements will be discussed again but with emphasis on new developments that are necessary for solving problems about 3D floating bodies.

3.1. Scheme for moving mesh

The main idea of dealing with mesh in the QALE-FEM is that the mesh is generated only once at the beginning of calculation and is moved at other time steps to conform to the motion of boundaries. The initial mesh can be unstructured and generated using an in-house mesh generator based on the mixed Delaunay triangulation and the advancing front technique (e.g. [56]) in this paper. To reflect the complexity of the fluid domain, one may assign different representative mesh size (*ds*) for different areas of the fluid domain to the mesh generator, which indicates the characteristic distance between two connected nodes. For example, near the free surface but far from the bodies, *ds* would be equal to about thirtieth of a wave length while it is reduced near the body surface, such as by half. Although *ds* is not precisely equal to the real mesh size, it largely indicates how fine the mesh is. It should be noted that the initial mesh can be generated using any

mesh generator with any degrees of complexity, either structured or unstructured, or even mixed. There is no limitation on the mesh structure for the QALE-FEM.

[Figure2]

Fig. 2. Illustration of the methodology for moving mesh

Obviously, the technique for moving the mesh is more crucial than generating the initial mesh in this method to achieve high robustness and high efficiency. For this purpose, a novel methodology has been suggested and adopted, in which interior nodes and boundary nodes are considered separately; and the nodes on the free surface and on rigid boundaries are considered separately. Furthermore, the nodes on the free surface and on the rigid boundaries are split into three groups: these on waterlines, these (inner-free-surface nodes) on the free surface but not on waterlines and these (inner-body-surface nodes) on the rigid boundaries but excluding those on waterlines. Different methods are employed for moving different nodes. The sequence and the method are illustrated in Fig. 2.

3.1.1 Moving interior nodes

To move the interior nodes which do not lie on boundaries, a spring analogy method is used. In this method, nodes are considered to be connected by springs and the whole mesh is then deformed like a spring system. Specifically, the nodal displacement is determined by

$$\Delta\vec{r}_i = \sum_{j=1}^{N_i} k_{ij}\Delta\vec{r}_j \Big/ \sum_{j=1}^{N_i} k_{ij} , \tag{23}$$

where $\Delta\vec{r}_i$ is the displacement of Node i; k_{ij} is the spring stiffness and N_i is the number of nodes that are connected to Node i. As pointed out in [47], the spring analogy method was originally adopted to cope with aerodynamic problems (e.g, [57-59]) without the free surface and without surface-piercing floating bodies. To apply it to the problems associated with the large deformation of the free surface, particularly together with the large motion of such floating bodies, the authors of this paper have modified the method considerably by proposing a robust and distinctive method for computing the spring stiffness:

$$k_{ij} = k_{ij}^0 \Psi^{fs} \Psi^{bs} \ , \tag{24}$$

where k_{ij}^0 is determined by

$$k_{ij}^0 = \frac{1}{l_{ij}^2} \tag{25}$$

with l_{ij} being the distance between Nodes i and j. Ψ^{fs} and Ψ^{bs} are the correction functions associated with the free surface and the moving rigid boundaries, respectively. These two functions are defined as

$$\Psi^{fs} = e^{\gamma_f \left[1+\left(z_i+z_j\right)/2d\right]} \ , \tag{26}$$

$$\Psi^{bs} = e^{\gamma_b (\hat{w}_i+\hat{w}_j/2)} \Big/ q_{\min}^{ij} \ , \tag{27}$$

where z_i and z_j are the vertical coordinates of Nodes i and j; d is the water depth; and γ_f is an coefficient that should be assigned a larger value if the springs are required to be stiffer at the free surface. It is found that $\gamma_f = 1.7$ is suitable for all the cases tested so far. $\hat{w}$ is a weight function given by,

$$\hat{w} = \begin{cases} 0 & d_f > D_f \\ 1 - d_f / D_f & d_f \le D_f \end{cases} \ , \tag{28}$$

where d_f is the minimum distance from the concerned node to the body surface as shown in Fig. 3; D_f is the distance between the body surface and the boundary of a near-body-region and is estimated by,

$$D_f = \varepsilon \min(B_b/2, L_b/2, D_r) \ , \tag{29}$$

where L_b, B_b and D_r are the length, breadth and draft of the body, respectively. Numerical tests show that the coefficient $\varepsilon = 1.5$ is suitable.

[Figure3]
Fig. 3. Region near moving body surface

The γ_b in the correction function Ψ^{bs} was chosen to be the same as γ_f in [18]. However, as well known, the curvature of the body surface, particularly in 3D cases, is an important factor to be considered when generating a good computational mesh, i.e., the areas with a larger curvature should have smaller elements. This kind of mesh may be easily generated at the first time step. However, such quality may not be retained during a long time simulation if the effect of curvature is not considered when moving the mesh. To take this effect into account, the γ_b is not chosen as a constant here; instead, it is evaluated by

$$r_b = \gamma_f \tilde{\omega}_{ij} \ , \tag{30a}$$

where $\tilde{\omega}_{ij}$ is a function related to the curvature of the body surface and is determined by

$$\tilde{\omega}_{ij} = \begin{cases} 1 & \mathrm{K}_{\max} = \mathrm{K}_{\min} \\ (\mathrm{K}_{ij} - \mathrm{K}_{\min})/(\mathrm{K}_{\max} - \mathrm{K}_{\min}) & \mathrm{K}_{\max} \neq \mathrm{K}_{\min} \end{cases} . \tag{30b}$$

In the equation, K is defined as

$$\mathrm{K} = \sqrt{\kappa_1^2 + \kappa_2^2} \ , \tag{31}$$

in which κ_1 and κ_2 are the curvatures of the intersecting curves between the body surface and each of two inter-perpendicular planes normal to the body surface at a node. $\mathrm{K}_{\max}$ and $\mathrm{K}_{\min}$ are, respectively, the maximum and minimum values of K at all nodes on the smooth part of body surfaces. K_{ij} is the value of K at a body-surface node that is the nearest to the centre of Spring *i*-*j*. It should be noted that the value of K at a node may vary with time since the node is continuously moving on the body surface; however, it is not necessarily updated at every time step because one just needs its approximate value to move the mesh. In fact, it is taken as the initial value calculated at the first time step in this paper, which works well. Nevertheless, it is envisaged that the value may need to be updated at a frequency of a certain number of steps for other cases considered in future and that there is no extra difficulty for doing so.

In addition, the motion of a 3D floating body may have 6 DoFs and thus the elements near body surfaces

generally undertakes a larger degree of distortion than those in 2D cases. To enhance the ability of resisting such distortion, $q_{\min}^{ij}$ is introduced in Eq. (27) for 3D cases, which is the minimum value of the quality indexes of all the elements sharing Spring *i*-*j*. The quality index for an element *e* is defined as (e.g. [55, 60]):

$$q_e = \frac{3R_i^e}{R_c^e} \tag{32}$$

where R_i and R_c are the inradius and circumradius of the element, respectively. This quality index is based on the fact that the best tetrahedronal element is a regular tetrahedron whose circumradius is three times its inradius (see, for example, [55, 60]). The range of the quality index is from 0 to 1. It equals to 1 for regular tetrahedrons and 0 for elements whose 4 points are located on a plane.

[Figure4]

Fig. 4. Region near waterlines

3.1.2 Moving nodes on waterlines and on the free surface

The positions of nodes on the free surface and waterlines are determined by physical boundary conditions, i.e., following the fluid particles, at most time steps. The nodes moved in this way may become too close to or too far from each other. To prevent this from happening, these nodes are relocated at a certain frequency, e.g., once every 40 time steps. However, it should be noted that the frequencies for relocating the nodes in different regions of the free surface and waterlines are not necessarily the same. Actually, it is found that the nodes in the near-waterline-region (those on the waterline of floating bodies and those on the free surface near the waterline, as shown in Fig. 4) often require higher frequency of redistribution in order to achieve high computational efficiency. For example, the nodes in the near-waterline-region are redistributed every 5 time steps while other inner-free-surface nodes may be redistributed once every 40 time steps.

When re-distributing the nodes on the waterline, a principle for a self-adaptive mesh is adopted, i.e., the weighted arc-segment lengths satisfy

$$\varpi_i \Delta s_i = C_s \tag{33}$$

where Δs_i is the length of i-th arc-segment between two successive nodes on the waterline and C_s is a constant. ϖ_i in the equation is a weighted function that may be related to the curvature of the waterline [47] but can be chosen as 1 based on all numerical tests so far.

In order to relocate the inner-free-surface nodes, two methods have been suggested. In the first method, the nodes are firstly projected on to a horizontal plane and then are moved using the spring analogy method in this plane, which results in new coordinates x and y. Using the new coordinates, the elevations of the free surface are evaluated by using an interpolating method as described in [23]. In order to take into account of the local gradient of the free surface and also the fact that the quality of mesh near floating body surfaces should be well preserved, the spring stiffness coefficients used for moving the nodes are different in x- and y-directions and given, respectively, by:

$$k_{ij}^{(x)} = \frac{1}{l_{ij}^2}\sqrt{1+\left(\frac{\partial \zeta}{\partial x}\right)^2}\, e^{\gamma_b(\hat{w}_i+\hat{w}_j/2)} \quad \text{and} \quad k_{ij}^{(y)} = \frac{1}{l_{ij}^2}\sqrt{1+\left(\frac{\partial \zeta}{\partial y}\right)^2}\, e^{\gamma_b(\hat{w}_i+\hat{w}_j/2)}, \tag{34}$$

where $\frac{\partial \zeta}{\partial x}$ and $\frac{\partial \zeta}{\partial y}$ are the local slopes of the free surface; and other parameters are the same as defined in Eq. (27). For brevity, this method is called MNPP (Moving Nodes in Projected Plane) method in this paper. Obviously, this method could not deal with the cases with multiple-valued surfaces, e.g., where overturning waves occurs. In those cases, the second method is suitable, which is the same as the one described in the following subsection for moving nodes on body surfaces.

3.1.3 Moving inner-body-surface nodes

Depending on shapes of floating bodies, the inner-body-surface nodes may be further split into three groups: these on wetted corners (submerged, intersecting points of two or more edges), these on edges and these on smooth parts of a body surface. Nodes on wetted corners are not moved relative to bodies. Nodes on edges are moved by using the spring analogy method for a line (special case of Eq. (24)) or by using Eq. (33). Both approaches are found to be satisfactory.

In order to redistribute the inner-body-surface nodes, a method similar to MNPP may be used. However, a floating body surface may become multiple-valued (more than one intersecting points between a vertical line and the body surface) due to large rotational motions, rendering the MNPP method inapplicable. To move nodes on such surfaces, another form of the spring analogy method is suggested here, which is based

on a local coordinate system formed by the local tangential lines and the normal line at the node concerned. In this local coordinate system, the surface is always single-valued, i.e., there is only one intersecting point between the body surface and a line parallel to the local normal line (of course, perpendicular to the local tangential lines). A node, e.g., i, is firstly moved along the tangential plane formed by tangential lines using

$$\Delta\vec{r}_{i\vec{\tau}_i} = \sum_{j=1}^{N_i} k_{ij}\Delta\vec{r}_{j\vec{\tau}_i} \Big/ \sum_{j=1}^{N_i} k_{ij} \,, \tag{35}$$

where $\Delta\vec{r}_{i\vec{\tau}_i}$ represents the tangential displacement of node i and N_i is the number of nodes connected to Node i. After that, the new position of the node on the body surface is found by interpolation in the local coordinate system, similar to that in the MNPP method. The spring stiffness in Eq. (35) is taken as $k_{ij} = 1/l_{ij}^2$. It is noted that the effects of body surface curvatures are implicitly taken into account even with such simple spring stiffness due to the use of the local coordinate system. For brevity, this method is called MNLTP (Moving Nodes in Local Tangential Plane) method in this paper.

The MNLTP method can also be used to move the inner-free-surface nodes but it is generally more computationally expensive than the MNPP method. Therefore, for the cases without overturning waves, the better choice should be the MNPP method; otherwise, the MNLTP method should be chosen to relocate the inner-free-surface nodes. Details are to be discussed in [34].

3.2. Calculation of fluid velocities on the free surface

The mesh used in the QALE-FEM may be arbitrarily unstructured and is continuously moving during the calculation. An effective method to calculate the fluid velocity on the free surface under this condition has been developed in [47] and used for problems about 2D floating bodies in [18]. The basic idea of this method is that the velocity at a node is split into normal and tangential components that are estimated separately. The normal component is computed by a three-point method and the tangential components are determined by using a least square method. This approach is also used for problems about 3D floating bodies. Details will not be repeated here and readers are referred to those two papers.

3.3. Calculation of fluid velocities on 3D body surfaces

The fluid velocities on body surfaces are required to calculate the pressure and to update the position of waterlines. The basic idea to calculate fluid velocity on body surfaces is similar to that mentioned above for

estimating the velocity on the free surface, i.e., the fluid velocity is split into the normal component and the tangential components. Nevertheless, the normal component on body surfaces is not necessarily estimated from the velocity potential because it must satisfy the boundary condition (Eq. 4). Actually, it can be determined by

$$\vec{v}_n = \vec{n} \cdot \vec{U}(t) = \vec{n} \cdot (\vec{U}_c + \vec{\Omega} \quad \vec{r}_b) . \tag{36}$$

After the normal component of the velocity is determined, a central difference scheme was applied to find the tangential velocity component at the inner-body-surface nodes in the cases for 2D floating bodies [18]. For the cases with 3D floating bodies considered here, the tangential velocity components at the inner-body-surface nodes are calculated using a least square method similar to that for the inner-free-surface nodes, in which each of equations is given by

$$\vec{v}_{\tau_1} \cdot \vec{l}_{IJ_k} + \vec{v}_{\tau_2} \cdot \vec{l}_{IJ_k} = \vec{l}_{IJ_k} \cdot \nabla\phi - \vec{v}_n \cdot \vec{l}_{IJ_k} \quad (k=1,2,3, \ldots\ldots, m) \tag{37}$$

where $\vec{l}_{IJ_k}$ is the unit vector from Node I to Node J_k that are neighbours of Node I on the body surface; $\vec{v}_{\tau_1}$ and $\vec{v}_{\tau_2}$ represent the velocity components in the tangential $\vec{\tau}_1$ and $\vec{\tau}_2$ directions, respectively. $\vec{\tau}_1$ and $\vec{\tau}_2$ can be any two vectors perpendicular to $\vec{n}$. For certainty, $\vec{\tau}_1$ is chosen to be $\vec{\tau}_1 = \vec{n} \quad \vec{e}_{xb}$ (or $\vec{\tau}_1 = \vec{n} \quad \vec{e}_{yb}$ if $\vec{n} \quad \vec{e}_{xb}$=0), where $\vec{e}_{xb}$ and $\vec{e}_{yb}$ are the unit vectors along x_b- and y_b- axes in the body-fixed coordinate system, while $\vec{\tau}_2$ is determined by $\vec{\tau}_2 = \vec{\tau}_1 \quad \vec{n}$.

However, at the nodes on the waterline, Eq. (37) become similar to a backward finite difference scheme due to unsymmetrical distribution of nodes about waterlines and so becomes less accurate. At such a node, a special treatment is adopted, i.e., the tangential velocity components are replaced by those along another two orthogonal vectors: one is tangent to the waterline (τ_w) and the other (n_w) is perpendicular to it but, of course, both are located in the plane tangential to the body surface at the node, as illustrated in Fig. 5. The velocity component $\vec{v}_{nw}$ in the direction of Vector $\vec{n}_w$ is estimated by using a three-point method:

$$\vec{v}_{nw} = \left[\frac{2}{3h_{I1}} \left(\frac{2h_{I1} + h_{I2}}{h_{I1} + h_{I2}} + \frac{1}{2} \right) \phi_I - \left(\frac{2}{3h_{I2}} + \frac{1}{h_{I1}} \right) \phi_{I1} + \frac{2}{3h_{I2}} \left(\frac{h_{I1}}{h_{I1} + h_{I2}} \right) \phi_{I2} \right] \vec{n}_w , \tag{38}$$

where *I1* and *I2* represent two points selected along the line $\vec{n}_w$, which is not necessarily coincided with any nodes; h_{I1} and h_{I2} are the distances between I and *I1* and between *I1* and *I2,* respectively*;* and ϕ_I, ϕ_{I1} and ϕ_{I2} denote the velocity potentials at Node I and the two points. The values of ϕ_{I1} and ϕ_{I2} are found by a

moving least square method (MLS) similar to that described in [61]. Eq. (38) is very similar to the equation for estimating the normal velocity on the free surface in [47].

[Figure5]

Fig. 5. Illustration of tangential and normal vectors of waterline

The velocity component $\vec{v}_{\tau w}$, in the direction of $\vec{\tau}_w$, can be computed by using Eq. (37) with $\vec{v}_{\tau_1}$ and $\vec{v}_{\tau_2}$ being replaced by $\vec{v}_{nw}$ and $\vec{v}_{\tau w}$, respectively. Only two neighbour nodes (J_1 and J_2) of Node I on the waterline is considered for this purpose. Therefore, Eq. (37) actually become a central difference scheme for determining the component $\vec{v}_{\tau w}$ if the segments from J_1 to J_2 are on a same straight line.

It should be noted the above method is only applicable for smooth body surfaces. If a body surface has some edges, particular care needs to be taken, depending on whether the edges intersect with the waterline. If an edge does not intersect with any waterline, the velocity at nodes on it is simply replaced by those in the elements nearby. If an edge does intersect with a waterline, the special treatment must be applied with considering that the formulation needs the velocity component of fluid along the edge and the velocity potential at the corner point where the waterline and the edge joint, in order to update the position of the corner point and the value of the velocity potential on it. The three-point method given in Eq. (38) is used to compute the velocity component. The velocity potential at this point is interpolated from surrounding free-surface nodes by using the moving least square method mentioned above.

3.4. ISITIMFB-M procedure

It has been noted above that there is a difficulty with solving the BVP for the term $\partial\phi/\partial t$ due to the fully nonlinear coupling between floating bodies and wave motions. As discussed in §1, four types of methods have been suggested in the literature to tackle the difficulty, which include the indirect method (Wu & Eatock Taylor [11, 16]), the mode-decomposition method (Vingi & Brevig [36], Koo & Kim, [17]), the Dalen & Tanizawa's method (Dalen [12]; Tanizawa [48]) and the iterative method (Cao, Beck & Schultz

[13]). In the indirect method, six auxiliary functions were introduced and thus the time derivative of the velocity potential is not explicitly required if the pressure on body surfaces is not of interest. (If the pressure is required, another BVP for $\partial\phi/\partial t$ may need to be solved after the body acceleration and velocity are obtained by using the auxiliary functions.) In the mode-decomposition method, the body acceleration is decomposed into several modes (7 modes in 3D cases). In both the methods, every mode or auxiliary function is found by solving a BVP similar to that for the velocity potential but under different boundary conditions, i.e., seven such BVPs to be solved. The matrixes for all the BVPs are the same and so the CPU time is almost the same as that for solving one BVP of this kind if a direct solution scheme (such as Gauss Elimination) is employed. However, the direct method is unlikely to be suitable for solving a linear algebraic system containing a very large number of unknowns, such as in the cases involving 3D floating bodies. In such cases, an iterative scheme for solving the linear algebraic system is much more efficient in terms of CPU time and storage requirement. When using an iterative scheme, solving each of the BVPs needs almost the same CPU time, even they have the same matrix. That means that the indirect method and the mode decomposition method may require considerably more CPU time due to the need of solving several extra BVPs. In the method proposed by Dalen and Tanizawa, the body accelerations are implicitly substituted by the Bernoulli's equations and thus the velocity potential and its time derivative are solved without the need of explicitly calculating accelerations of the floating bodies. However, this method results in a special matrix for $\partial\phi/\partial t$ which is different from the one for the velocity potential and whose properties have not been sufficiently studied. This is likely to increase the difficulty for solving the algebraic equations associated with $\partial\phi/\partial t$ and also needs more CPU time for generating such a special matrix. That would be the main reason for this method not to be commonly used. In the iterative procedure for dealing with the full coupling, suggested by Cao, Beck & Schultz [13], the acceleration and velocity of bodies are explicitly and iteratively calculated at each time step; in this way, the need to solve extra equations in the first two methods and the problem with the third method is eliminated. It is noted that for the purpose of time marching, a standard explicit 4^{th}-order Runge-Kutta scheme is generally used in all these methods, which requires extra three sub-step calculations at one time step forward. In each sub-step, the geometry of the computational domain may or may not be updated. If it is not updated, it is called a frozen coefficient method; otherwise, it is called a fully updated method. The CPU time spent on updating in the fully updated method is roughly

equal to 4 times that in the frozen coefficient method. However, the frozen coefficient method may not lead to stable and reasonable results for problems about large motions of floating bodies, as indicated by Koo & Kim [17]. It is also noted that the body velocity is estimated from the acceleration at previous time steps in all the above methods; i.e., the corresponding time marching procedure is explicit, which may degrade the accuracy and even lead to instability unless sufficient small time steps are used.

The authors of this paper have developed an iterative method called ISITIMFB (Iterative Semi Implicit Time Integration Method for Floating Bodies) procedure in [18]. The distinct feature of this procedure is that body velocities are estimated implicitly and iteratively by considering the acceleration at both the previous and current time steps. This feature enables one to use relative larger time step without the need of sub-step calculations. As demonstrated by numerical tests by Yan & Ma [18], the ISITIMFB procedure is accurate, stable and efficient, and is the best one matching the QALE-FEM. In this paper it is still adopted but some modification is made to further improve its efficiency.

The basic idea of the modification is to update more parameters implicitly and iteratively. As is known, apart from body velocities, the positions of and the velocity potential on the free surface are also updated in the time marching procedure. In the ISITIMFB procedure, they are obtained at each time step by explicitly integrating Eq. (2) and Eq. (3), respectively. For the same reason to use implicit scheme for updating body velocities, it is also better to update the above two physical quantities implicitly. However, if the positions of the free surface are updated implicitly, more CPU time is spent not only on finding the new free surface but also on forming the new coefficient matrix for Eq. (21) during the iteration. Considering these factors, the ISITIFMB procedure is modified by including implicit and iterative update of the velocity potential on the free surface in addition to dealing with the body velocity in such a way in the paper. The modified ISITIFMB procedure (referred as ISITIMFB-M) is described as follows.

Suppose that all calculations until $t=t_{n-1}$ (n>0) have been completed, and so the velocity on the free surface and the positions of all boundaries including the free surface and the body surface have been obtained. The computation at time t_n is performed by the following procedure:

1) Predict the body acceleration $\vec{A}^{n(0)}$ by a curve fitting of accelerations ($\vec{A}_b^{n-1}$ and $\vec{A}_b^{n-2}$) at previous time steps using a least square method and then estimate the corresponding body velocity by using the Adams-Moulton method [62], its order of accuracy being $O\left(\Delta t^4\right)$, as follows,

$$\vec{U}_b^{n(0)} = \vec{U}_b^{n-1} + \frac{\Delta t}{12}(5\vec{A}_b^{n(0)} + 8\vec{A}_b^{n-1} - \vec{A}_b^{n-2}), \tag{39}$$

where $\vec{U}_b^{n-1}$ is the velocity at the previous time step and $\vec{U}_b^{n(0)}$ represents the predicted velocity for the current time step, which is used as the initial values of iteration. Here the velocity and the acceleration include translational and rotational components.

2) Predict the velocity potential on the free surface for this time step using the scheme in [23],

$$\phi_{sf}^{n(0)} = \phi_{sf}^{n-1} + \left[3\left(\frac{D\phi}{Dt}\right)^{n-1} - \left(\frac{D\phi}{Dt}\right)^{n-2}\right]\frac{\Delta t}{2} \tag{40}$$

3) Solve the BVP for ϕ using $\vec{U}_b^{n(0)}$ in Eq. (4) for the boundary condition on the body surface and $\phi_{sf}^{n(0)}$ for the boundary condition on the free surface.

4) Calculate the fluid velocity, and then $\left(\frac{\partial\phi}{\partial t}\right)^{n(0)}$ as well as $\left(\frac{D\phi}{Dt}\right)^{n(0)}$ on the free surface.

5) Calculate the fluid velocity $\vec{V}_b^{n(0)}$ on the body surface.

6) Using the following loop to refine the solution:

(a) Solve the BVP for $\left(\frac{\partial\phi}{\partial t}\right)^{n(k)}$ using $\vec{A}^{n(k-1)}$, $\vec{U}_b^{n(k-1)}$ and $V_b^{n(k-1)}$ in its boundary condition on the body surface (Eq. (17) and $\left(\frac{\partial\phi}{\partial t}\right)^{n(k-1)}$ for its boundary condition on the free surface (Eq.16)), where the subscript $n(k\text{-}1)$ indicates the variables at time t_n but at k-th iteration (k=1,2,3……) in the loop;

(b) Calculate the forces or moments (generally represented by $\vec{F}^{n(k)}$) and then the acceleration by

$$\vec{A}_b^{n(k)} = [M]^{-1}\left[\alpha^n \vec{F}^{n(k)} + (1-\alpha^n)\vec{F}^{n(k-1)}\right], \tag{41}$$

in which the mass matrix $[M]$ should be changed to the matrix of the inertia moment $[I]$ if the angular acceleration is concerned. α^n is a relaxation coefficient determined in the same way as in [18].

(c) Estimate the new body velocity using the similar method to Eq. (39) but with the new value of the acceleration $\vec{A}_b^{n(k)}$:

$$\vec{U}_b^{n(k)} = \vec{U}_b^{n-1} + \frac{\Delta t}{12}(5\vec{A}_b^{n(k)} + 8\vec{A}_b^{n-1} - \vec{A}_b^{n-2}); \tag{42}$$

(d) Update the velocity potential on the free surface using,

$$\phi_{sf}^{n(k)} = \phi_{sf}^{n-1} + \frac{\Delta t}{12}\left[5\left(\frac{D\phi}{Dt}\right)^{n(k-1)} + 8\left(\frac{D\phi}{Dt}\right)^{n-1} - \left(\frac{D\phi}{Dt}\right)^{n-2}\right] \tag{43}$$

(e) Solve the BVP for ϕ using the new body velocity $\vec{U}_b^{n(k)}$ in Eq. (4) for the boundary condition on the body surface and the new potential value $\phi_{sf}^{n(k)}$ for the boundary condition on the free surface;

(f) Calculate the fluid velocity, and then $\left(\frac{\partial\phi}{\partial t}\right)^{n(k)}$ as well as $\left(\frac{D\phi}{Dt}\right)^{n(k)}$ on the free surface

(g) Calculate the fluid velocity $\vec{V}_b^{n(k)}$ on the body surface;

(h) Check if the relative error of accelerations (or forces) is small enough; if not, go to a); otherwise go to 7).

7) Update the position of the body using the final body velocity and acceleration in the above loop by using the 3rd order Taylor expansion,

$$\vec{S}_b{}^{n+1} = \vec{S}_b{}^{n} + \vec{U}^{n(u)}\Delta t + \frac{\Delta t^2}{2}\dot{\vec{U}}^{n(u)} + \frac{\Delta t^3}{6}\frac{d\dot{\vec{U}}^{n(u)}}{dt} \tag{44}$$

where $\vec{S}_b{}^{n+1}$ is the translational or angular displacement of the body used for the calculation of the next time step; $\vec{U}^{n(u)}$ and $\dot{\vec{U}}^{n(u)}$ represent the final values of body velocities and accelerations (translational or angular) in the above loop, respectively; and $\frac{d\dot{\vec{U}}^{n(u)}}{dt}$ is calculated by using the finite difference scheme, i.e., $\frac{d\dot{\vec{U}}^{n(u)}}{dt} = \left(\dot{\vec{U}}^{n(u)} - \dot{\vec{U}}^{n-1(u)}\right)\Big/\Delta t$.

8) Update the positions of the free surface using the same method as in [23].

9) Go to next time step.

Compared to ISITIMFB, the ISITIMFB-M procedure includes two extra steps: 6(d) and 6(f). The efficiency of the iterative procedure is signified by the iteration counter in the above loop. For a given accuracy requirement, time step and wave/body oscillating period, the iteration counter depends on the quality of the predicted values of the acceleration, the velocity, the velocity potential and its time derivative. These two extra steps in the loop help give better prediction to all the parameters and so reduce the iteration counter. Of course, introducing the two extra steps inevitably increases the computational time for each

iteration. However, the increase in the CPU time due to them is insignificant according to the numerical tests. Consequently, as long as the iteration counter in the ISITIMFB-M procedure is less than that for the original one, its overall efficiency should be improved. More discussion will be given in §4.4. The control error (accuracy requirement) in Step 6(h) is chosen as 0.5% based on numerical tests carried out in [18] and on the cases presented in this paper (details about this will not be given here as they are similar to those in [18]). In the end, it is noted that the iteration is not necessary for problems about fixed bodies or those with forced motions.

[Figure6]

Fig. 6. Illustration of the initial mesh near a 3D floating body

4. Validation and convergence tests

The QALE-FEM has been validated in various cases including 2D waves [47], interaction between waves and 2D floating bodies [18] and 3D overturning waves [34] by using various available results. In this section, the method newly extended to problems about 3D floating bodies will be validated by comparing its numerical predictions with some experimental results from other papers. Its convergent properties are also investigated here. Due to the fact that availability of experimental data for general 3D floating bodies with 6-DoFs motions in steep waves is very limited in the public domain, only two special cases are selected for the purpose of validation: a SPAR platform and a barge-type floating body. Nevertheless, one may agree that investigations on these two quite different cases should shed significant light on whether the method is reliable and accurate.

All the investigations below are carried out by using a numerical tank where a damping zone together with Sommerfeld condition is applied to absorb the reflection from the far end wall [23], as mentioned before. It should be noted that in 3D cases the reflection from the side walls is also unexpected. One may

use similar technique to absorb the reflection from the side walls. Nevertheless, a sufficient wide tank is applied in this paper to eliminate these effects, rather than making much effort on the absorbing techniques. The initial mesh to be used is unstructured near the body, as illustrated in Fig. 6.

In the rest of the paper, the parameters with a length scale are nondimensionalised by the water depth d; and other parameters by ρ, g and d, such as the time (t), frequency (ω) and forces (F) becoming

$$t \to \tau\sqrt{d/g}\ ,\ \omega \to \omega\sqrt{g/d}\ \text{ and }\ F \to f\rho g d^3\ ,$$

unless mentioned otherwise. Sometime, the wave length determined by using the linear wave dispersive relation, $\lambda = \frac{2\pi}{\omega^2}\tanh(2\pi/\lambda)$, is used as a characteristic length. The motion of the wavemaker is specified as $-a\cos(\omega\tau)$ for generating monochromatic waves or as $-a_1\cos(\omega_1\tau) - a_2\cos(\omega_2\tau)$ for bichromatic waves.

4.1. Responses of a moored SPAR platform

A SPAR platform is basically a large vertical cylindrical floating structure which may be moored by mooring lines to the sea bed. For the SPAR platform considered here, the diameter is 0.135; the initial draft is 0.6607; the mass and the radius of gyration (pitch and roll) are 0.005926 and 0.2078, respectively. The centre of gravity from its keel is 0.308 and the fairlead of mooring lines from its keel is 0.3087. The mooring line is considered as a nonlinear spring with its stiffness taken as 2.163×10^{-4} up to an offset of 0.04567 and 4.512×10^{-4} beyond it. Two cases are considered here. In the first one, a monochromatic wave with the amplitude of 0.02 and the period of 1.7 is generated while in the second one, the body is subjected to a bichromatic wave with the amplitudes and periods being (0.02, 0.02) and (1.943, 2.125), respectively. The cases are the same as in [54] and [63]. The length and width of the numerical tank are taken as L=8 and B=2. The mesh is unstructured with the representative mesh size on the free surface but not near the body being specified by $ds \approx \lambda/30$ (roughly 30 nodes in a wavelength). The time step is taken as T/128, where T is the wave period defined by $2\pi/\omega$. Figs. 7 and 8 show, respectively, the comparison of the pitch motions of the SPAR platform subjected to the monochromatic wave and the bichromatic wave, which are obtained by the QALE-FEM and experiments (Weggel et al [63]).

[Figure7]

Fig. 7. Comparison between numerical and experimental results for the pitch of a SPAR subjected to a monochromatic wave (experimental data are from Weggel et al [63])

[Figure8]

Fig. 8. Comparison between numerical and experimental results for the pitch of a SPAR subjected to a bichromatic wave (experimental data are from Weggel et al [63])

[Figure9]

Fig. 9. Comparison of the pitch of a SPAR in tanks with different widths

As can be seen, the numerical results obtained by the QALE-FEM agree reasonably well with the experimental data in both cases. The same level of agreement for surge motions has also been achieved, though the figure is not given here for brevity.

An investigation is made on the effects of side walls, in which the width of the tank is extended to 3. The comparison of the responses of the SPAR platform corresponding to two widths is shown in Fig. 9, where the numerical result for the case with B=2 is the same as that shown in Fig. 8. From this figure, it is observed that the difference between the results for B=*2* and B=*3* are very small. This means that B=*2* is sufficient wide for this case in the duration of the simulation.

4.2 RAOs of surge, heave and pitch of a barge-type floating body

Only the waves with two specified frequencies in cases shown in Figures 7 and 8 are considered. As is well known, incident waves with different frequencies may lead to different responses of a floating body. In order to further validate the QALE-FEM for the cases with incident waves of various frequencies, the RAO (response amplitude of operator) of a barge-type floating body are investigated in this sub-section.

For this purpose, the QALE-FEM is applied to a similar case in experiments on a barge-type floating body by Shashikala, Sundaravadivelu & Ganapathy [64]. These experiments were carried out in a tank with water depth of 2.35m. Based on this, other parameters nondimensionlised by the water depth are chosen as follows. For the barge-type floating body, the length (L_b), breadth (B_b) and draft (D_r) are taken as 0.8511, 0.1702 and 0.04255, respectively; its mass is 6.164×10^{-4} and its centre of gravity above base (KG) is 0.03829; its moment of inertia about longitudinal, transverse and vertical axis are 2.344×10^{-4} , 5.326×10^{-4} and 5.326×10^{-4} , respectively. A mooring line with the stiffness of 0.1846 is attached on the body with a distance of 0.03404 above the centre of gravity. The measured natural frequency for surge, heave and pitch are 5.475, 3.408 and 3.074, respectively. The RAOs in the experiments are determined by the amplitudes of motions in the steady state divided by the wave amplitude. In the numerical simulation, the RAOs are estimated by performing FFT analysis on the steady-state portion of the time histories of corresponding motions. The cases presented in this subsection are simulated in a numerical tank with L=9 and B=2. Numerical testes are also carried out in wider tanks but do not show significant difference from the results presented here. The computational mesh is unstructured with about 30 nodes in each wave length on the free surface but away from the body and with the representative mesh size near the body being about half of that in the other area. The wavemaker is located at x= -5 initially. The amplitudes of the wavemaker are adjusted properly so that the generated incident wave steepness (wave height/wavelength) is about 0.02. The time step is taken as T/128.

[Figure10a]

Fig. 10 (a) Surge RAO

[Figure10b]

Fig. 10 (b) Heave RAO

[Figure10c]

Fig. 10 (c) Pitch RAO

Fig. 10. Comparison of responses of a floating barge in regular waves
(Experimental data are from Shashikala et al [64])

The RAOs of surge, heave and pitch motions corresponding to different incident waves as a function of $\omega^* = \omega^2 L_b / 2$ are plotted in Fig. 10, together with the experimental data from Shashikala et al [64]. It can be found from this figure that the present numerical results generally agree well with experimental data in a

wide range of frequencies, though visible discrepancies at some points inevitably exist.

4.3. Discussion on convergence

In above subsections, the QALE-FEM for the responses of 3D moored floating bodies has been validated using two different cases by specifying a time step and a mesh size. Reasonable agreement with experimental data has been achieved. However, one may wonder what would happen if other values of time steps and mesh sizes are used. In this sub-section, the convergence properties in the cases with a 3D floating body are discussed in order to shed some light on whether the time steps and mesh sizes used above are appropriate and also on the choice of these parameters in other calculations. Although similar investigations have been carried for all the cases discussed above, only those corresponding to Figure 8 are present here.

[Figure11a]

(a) different time steps

[Figure11b]

(b) different mesh sizes

Fig. 11. Tome histories of pitch obtained by using different time steps and mesh sizes

For this purpose of investing the effect of time steps, they are chosen as *T*/200, *T*/128 and *T*/64 respectively. For all these time steps, the representative mesh size is roughly $\lambda/30$. Fig. 11 (a) shows the time history of pitch obtained by using different time steps for the same case in Fig. 8. It is observed that the results appear to be the same when the time step is smaller than *T*/128; while the result for the case with the time step of *T*/64 is slightly different from the results of other two cases. The relative difference is about 1%, which is estimated by using the same method in [18]. This implies that a time step of *T*/64 may also be acceptable. To investigate the effect of mesh sizes, the time step is taken as *T*/128 and the representative

mesh sizes are specified as $\lambda/40$ (the number of elements: 1,663,276) , $\lambda/30$ (the number of elements: 739,247) and $\lambda/20$ (the number of elements: 337,764), respectively. Fig. 11(b) shows the time history of pitch obtained by using the different mesh sizes. It can be seen that the difference between the results obtained by the mesh sizes of $\lambda/30$ and $\lambda/40$ is negligible but the result obtained by the mesh size of $\lambda/20$ is different from other two. This implies that in the 3D case, the mesh size should be smaller than $\lambda/30$.

These investigations seems to suggest that time steps (*T*/128) and mesh sizes ($\lambda/30$) selected for above validation are appropriate. Nevertheless, it should be noted that the investigations on how numerical results are related only to mesh sizes without considering mesh structures may not be considered as complete because the results depend on both. However, it is impractical to consider all possible mesh structures as the unstructured meshes are used in this paper and that the mesh sizes constantly change with time due to the motions of the free surface and floating bodies. Therefore, mesh sizes used above should only be considered as an indicator of different meshes. It should also be noted that the minimum time steps and mesh sizes for a specified error may also depend on the motion of floating bodies, wave amplitudes and so on. Considering these uncertainties, the conclusion about the selection of time steps and mesh sizes may not hold for general cases, though it would be considered as a good indication. On this basis, the results for all the cases presented in §5 have been validated by using different time steps and mesh sizes, though the results obtained by only using *T*/128 for the time step and $\lambda/30$ for the mesh size are presented.

4.4. Comparison between ISITIMFB-M and ISITIMFB procedures

In this paper, the ISITIMFB procedure has been modified into the ISITIMFB-M procedure. The efficiency of the ISITIMFB compared to the mode-decomposition method with the 4th-order Runge-Kutta scheme has been discussed in [18] for 2D floating body problems. The latter needs to solve 20 BVPs in one step forward in those cases. It was concluded that the ISITIMFB was more efficient as long as the average iteration counter in the ISITIMFB in one step forward was smaller than 10. In 3D cases, the mode-decomposition method with the 4th-order Runge-Kutta scheme may need to solve 32 BVPs in one step forward, implying that our iterative procedure would be more efficient if the average iteration counter is smaller than 16 in one step forward. The smaller the counter, the more efficient the procedure is.

As has been discussed in §3.4, it is expected that the new ISITIMFB-M procedure would require a fewer

iteration counter than the ISITIMFB. In the current sub-section, this will be shown by comparing the average iteration counters required by two procedures. Because the iteration counters depend on both time steps and natural frequencies of floating bodies as pointed out in [18], the comparison is made by looking at both the effects. The change of natural frequencies is achieved by varying the mass of the body with other parameters remaining the same.

The case used here is the same as that used for investigating the properties of the ISITIMFB in [18] but the 2D barge-type body is projected along *y*-direction to form a 3D body. The dimensional water depth is the same as the characteristic wave length (λ). The frequency of the incident wave is specified by $\xi = \omega^2 B_b / 2 = 0.4$ and the dimensionless wave height generated is about 0.018. For this body, the width (B_b) is 0.1273; the draft (D_r) is 0.06366; the gravitational centre is located at 0.02929 from the keel of the barge. The mooring line is modelled by a horizontal spring through the gravitational centre with the spring stiffness taken as 7.188×10^{-4}. This case is run in a nondimensionalised numerical tank with $L \approx 13$ and B=0.3. The initial mesh used is unstructured with about 35 elements on the free surface in each wavelength.

[Figure12]

Fig. 12. Average iteration counters in one step forward corresponding to different time steps

The average iteration counters in one step forward corresponding to different time steps are shown in Fig.12. with the mass (m_0) being 1.135×10^{-3} and the moment of inertia about the gravitational centre is 2.384×10^{-6}. In the figure, there are two rows of numbers under the horizontal axis. The first row represents the number of time steps in each wave period and the second row gives the value of the time step, i.e. the period divided by the number in the first row. As could be seen, the average iteration counter for the ISITIMFB-M procedure is not larger than 5 for this case and is averagely about 26% less than that for the ISITIMFB procedure in the same situation.

Fig. 13 shows the iteration counters corresponding to a range ($0.1 \le m/m_0 \le 100$) of the body mass with the mooring stiffness and the shape of the floating body remaining the same, resulting in different natural frequencies. The time step is taken as $T/128$ and all other parameters are the same as those in Fig. 12. Again, the iteration counter of the ISITIMFB-M procedure is generally significantly smaller than that of the ISITIMFB procedure. It is noted that the iteration counter for the ISITIMFB procedure are different from that published in [18]. That is because the computer code is further optimized here.

The iterative counters may be problem-dependent. Nevertheless, for problems about floating bodies of different configurations presented in §5, the iteration counter for the ISITIMFB-M procedure never exceeds 10, actually less than 7 in most of the cases. This may indicate that the ISITIMFB-M procedure is more efficient than the mode-decomposition method with the 4th-order Runge-Kutta scheme if the latter would have been used in the QALE-FEM.

[Figure13]

Fig. 13 Average iteration counters in one step forward corresponding to different masses (dt = T/128 and m_0=1.135×10^{-3})

5. **Numerical results for 3D floating bodies and discussions**

One of distinctive aspects of this paper is to present some numerical results for one or two floating bodies, freely responding with up to 6 DoFs to the excitation of waves, obtained by the QALE-FEM based on the fully nonlinear and full coupling theory. Although the QALE-FEM can be applied to any form of floating bodies, Wigley Hulls are selected as a representative because it is easier for parameter studies and also because it is similar to many practical floating bodies, such as FPSOs and LNG (Liquefied Natural Gas) carriers, in terms of their composite shapes composed of smooth surfaces and sharp edges piercing the free surface. As pointed out before, although the method is based on the potential theory, the viscous effects on the motions of floating bodies may be modelled by adding empirical damping in the dynamic equations of

floating bodies. This is a usual approach in ship dynamics when the potential theory is applied. To show this flexibility, an artificial viscous damping is added in all the motion components in this section, for which the damping coefficient is specified as 0.1% of the critical damping in each component. All the results presented in this section are obtained by using a time step of T/128 and a representative mesh size of λ/30 unless mentioned otherwise. However, as pointed out before, these results have been checked with smaller time steps and mesh sizes.

5.1. Single Wigley Hull floating over a flat seabed

The shape of the Wigley Hull used here is expressed as

$$\eta = (1-\varsigma^2)(1-\xi^2)(1+0.2\xi^2) + \varsigma^2(1-\varsigma^8)(1-\xi^2)^3, \tag{50}$$

where

$$\xi = 2x/L_b, \eta = 2y/B_b, \varsigma = z/D_r \tag{51}$$

and L_b, B_b, D_r are the length, breadth and draft of the Wigley Hull. To make more sense, forces and moments are nondimensionlised in this subsection by using different quantities: forces by $\rho g \forall$ (where $\forall$ is the volume of the submerged part of the hull), the pitch and yaw moments by $\rho g \forall L_b$ and the roll moment by $\rho g \forall B_b$. Other parameters are nondimensionlised in the same way as above.

As indicated by Yan & Ma [18] for 2D floating body cases, the amplitudes of motions in the transient period may be considerably larger than those in the steady state and depend on natural frequencies of floating bodies. The corresponding characteristics of 3D floating bodies are discussed here.

For this purpose, a Wigley Hull in a head sea with L_b=1.0, B_b=0.2 and D_r=0.15 is considered. This is referred as 'Hull-1L'. The dimensionless mass and the pitch moment of inertia are taken as 0.01677 and 0.00875, respectively. The centre of gravity is located at 0.025 above its keel. Two mooring lines are connected to the bow and the stern of the Wigley Hull, respectively, in the longitudinal direction and at the water level initially. The spring stiffness of the mooring lines is taken as 0.015. Without considering the added mass, the natural frequencies of surge, heave and pitch are roughly 1.3355, 3.1666 and 1.3363, respectively. The numerical tank for these cases has the length of 15 and the width of 6. The incident wave is generated by the piston wavemaker located at x= -8 with the amplitude (a) of 0.05 and frequency (ω) of 1.7691. The characteristic wavelength (λ) is about 2, twice the length of the Wigley Hull. The wave

steepness is about 0.088. Numerical tests have been carried out for this configuration by using a wider tank and indicate that the reflection from the side walls is negligible when $\tau < 100$.

[Figure14]

Fig. 14 Snapshots of the part of the free surface near the body at (a) $\tau \approx 27.69$ and (b) $\tau \approx 61.78$ (a=0.05, $\omega = 1.7691$, k_m=0.015, L=15, B=8)

Fig. 14 shows some snapshots of the wave elevation and the body motion at a transient instant and in the nearly-steady state. Fig. 15 gives the time history of the pitch motion. One may see from this figure that the maximum transient pitch motion is much larger than the amplitude in the steady state, the latter being usually estimated by using the RAOs in engineering practice. Similar property is also observed for the surge motion but not shown here. This implies that the transient responses rather than RAOs should be considered in design in order to determine the maximum motion of a floating body subjected to a transient wave. Due to this fact, presentations in the following subsections focus on the transient effects.

[Figure15]

Fig. 15 Time history of pitch motion (a=0.05, $\omega = 1.7691$, k_m=0.015, L=15, B=8)

[Figure16a]

Fig. 16 (a) surge force

[Figure16b]

Fig. 16 (b) heave force

Fig. 16 Hydrodynamic forces acting on the Wigley Hull in cases with different wave amplitudes (a=0.05, $\omega = 1.7691$, k_m=0.015, L=15, B=8)

To show the effect of nonlinearity, the dimensionless hydrodynamic forces, divided by the dimensionless wavemaker amplitude a, acting on the floating body are plotted in Fig. 16 for two cases with a=0.004 and a=0.05. It can be observed that the ratio of the surge force amplitude to the wavemaker amplitude (and so the wave amplitude) tends to decrease as the increase of the later in the steady state. The profile of the surge force in the case with the steeper wave (a=0.05) is not symmetric about the apex point in one wave period. On the other hand, the ratio of the heave force for the larger wave amplitude has a significantly larger transient value and a more complicated profile, though the steady amplitude does not exhibit considerable difference (Fig. 16(b)). This indicates that design based on the forces estimated by using a linear or even second order theory in frequency domain may not be safe as they could only predict the amplitude in steady states.

[Figure17]

Fig. 17 Relative run-up recorded at the bow of the hull (a=0.05, $\omega = 1.7691$, k_m=0.015, L=15, B=8)

Apart from the forces, the relative run-up, which is defined as the displacement of the waterline at a point measured in the vertical direction of the body-fixed coordinate system, is also of interest for design of floating bodies and is useful for predicting the possibility of green water occurrence. The relative run-up (η_k) at the bow is plotted in Fig. 17 for the same case in Fig. 16. It obviously shows that the shape of the run-up history becomes unsymmetrical about the apex points and more importantly that the highest run-up for the case with the larger amplitude is considerable larger than that would be predicted by a linear theory.

The later may just result in no green water when the phenomenon actually happens.

[Figure18]

Fig. 18 Responses of the Wigley Hull for different spring stiffness of mooring lines (a=0.05 and $\omega = 1.7691$)

It could be understood that the transient characteristics may be affected by the natural frequency of floating bodies. This will be demonstrated by the same case as above with different spring stiffness of the mooring lines. To do so, another case with k_m = 0.00025 is selected. Without considering the added mass, the corresponding natural frequencies of surge, heave and pitch for this case are roughly 0.545, 2.9225 and 1.0133, respectively. All other parameters are the same as those in Fig. 15. The comparison of the responses of the hull associated with different stiffness are depicted in Fig. 18, where the time histories for k_m = 0.015 shown in Fig. 15 are re-plotted. This figure illustrates a feature that the transient responses are considerably different for different natural frequencies. For example, the maximum oscillating amplitude of the transient pitch motion for k_m = 0.015 is significantly larger than the steady amplitude while for k_m = 0.00025 both are almost the same. That may be because the natural frequency of pitch in the former case is closer to the incident wave frequency than that in the latter case. In addition, there is an evident drift

motion in surge direction for k_m = 0.00025. This is caused by the steady drift force which has a larger effect in the second case where the spring representing the mooring lines is softer.

[Figure19]

Fig. 19 Pitch and surge motions of Wigley Hulls with different hull sizes (a=0.05 and $\omega = 1.7691$)

Another factor that may affect the responses of a floating body is its sizes. In order to investigate this effect, other two Wigley Hulls apart from Hull-1L are considered. They are 'Hull-2L' with L_b=2.0, B_b=0.4 and D_r=0.2; and 'Hull-3L' with L_b=3.0, B_b=0.6 and D_r=0.3. For the Hull-2L, the spring stiffness of the mooring lines, the mass and pitch moment of inertia are taken as 0.08, 0.089442 and 0.15634, respectively. For Hull-3L, they are 0.27, 0.30234 and 1.0237, respectively. Using these parameters, Hull-2L and Hull-3L have the same natural frequencies as Hull-1L if the added mass is ignored. All other parameters are the same as those in the case for Fig. 14 and thus the lengths of Hull-1L, Hull-2L and Hull-3L are roughly equal to 0.5λ, 1.0λ and 1.5λ, respectively. The responses of these three Wigley Hulls are plotted in Fig. 19 and Fig. 20. It is seen that transient and steady amplitudes of the surge (Fig. 19a) and pitch motion (Fig. 19b) are considerably reduced as the increase of the hull sizes while the heave motions of Hull-2L and Hull-3L in Fig. 20 are much smaller than that of the Hull-1L but themselves are quite similar. On the other hand, these observations imply that the transient behaviour of a floating body with given sizes may be different in different waves.

[Figure20]

Fig. 20 Heave motion of Wigley Hulls with different hull sizes (a=0.05 and $\omega = 1.7691$)

It should be noted at the end of this subsection that the specific values of transient amplitudes may be different from what have been shown above if the real damping for the bodies are used. Nevertheless, these cases clearly demonstrate that transient phenomena should not be ignored without careful investigations, particularly by using methods based on fully nonlinear theory.

5.2 Single Wigley Hull floating over a complex seabed

In many applications, one can see structures floating in a shallow water region, such as offshore LNG terminals and floating oil storage bases. For those floating bodies, the effects of the local bathymetry of the seabed should be considered. Yan & Ma [19] studied effects of the seabed on 2D floating bodies using the QALE-FEM. In this subsection, the method is applied to study the behaviours of a single Wigley hull floating near a bump on the seabed. The bump is expressed as

$$Z(x', y') = \begin{cases} z_{sb}\left[1-(x')^2-(y')^2\right]^{\alpha_{sb}} & x'<1,\ y'<1,\ 1-(x')^2-(y')^2>0 \\ 0 & \text{otherwise} \end{cases} \tag{52a}$$

$$x' = |x - x_c| / r_x \tag{52b}$$

$$y' = |y - y_c| / r_y \tag{52c}$$

where (x_c, y_c) is the centre of the bump, z_{sb} is its maximum height, and r_x, r_y and α_{sb} are coefficients.

[Figure21]

Fig. 21 Example of a seabed geometry (z_{sb} =0.7, $r_x = 7, r_y = 3, \alpha_{sb} = 1$)

Specifically, a bump, centred at x_c=-0.5 and y_c =3, with z_{sb} =0.7, $r_x = 7, r_y = 3$ and $\alpha_{sb} = 1$as shown in Fig. 21 is considered, which is in a tank with the length of 15 and width of 6. In addition, this bump is adjacent to a vertical wall at y=3, making a situation similar to that a floating body is moored to a position near a coastal wall. The amplitude and frequency of the wavemaker are 0.03 and 1.7691, respectively. These yield a wave steepness of about 0.058. The Wigley hull is centred at x=0, and y=2, i.e., the distance between the hull centre and the wall at y=3 is d_b =1. The mass of the hull is 0.01677 and its inertia moments of roll, pitch and yaw are taken as, 0.003282, 0.00875 and 0.025, respectively. Thus the natural frequencies of surge, heave and pitch are the same as before and the natural frequencies of roll, yaw and sway are 1.2883, 0.5477 and 1.3355 without considering added masses and moments. Other parameters are the same as those for the case in Figs. 14-17.

[Figure22]

Fig.22 Comparison of the free surface in cases with (a) or without the bump (b)
(z_{sb} =0.7, $r_x = 7, r_y = 3$, $\alpha_{sb} = 1$, $\omega = 1.7691$, a=0.03 $\tau \approx 50.17$)

Fig. 22 shows a snapshot for this case (Fig.22a) and for the case (Fig.22b) without a bump on the seabed but all others being the same. This figure clearly demonstrates that the wave in the former case is significantly different from that in the latter case. Particularly, the wave in the former evolves into short-crested after the body, while the wave in the latter still remains to be long-crested. In addition, the wave near the wall for the case with the bump becomes shorter, higher and so steeper than the wave for the case without the bump. This phenomenon can be seen more evidently in Fig. 23, where the wave profiles at the wall (y=3) for the two cases are compared. Because the wave becomes shorter, one can deduce that the celerity of the wave near the shore becomes less, which is consistent with the fact pointed out by Grilli & Horrillo [65] that the wave celerity reduces as a result of decreasing water depth.

[Figure23]

Fig. 23 Wave profiles at y=3 and $\tau \approx 36.92$ (z_{sb} =0.7, $r_x = 7, r_y = 3$, $\alpha_{sb} = 1$, $\omega = 1.7691$, a=0.03)

The features discussed above are obviously related to the height of the bump (z_{sb}). To investigate the effects of z_{sb}, another two cases with z_{sb} =0.35 and z_{sb} =0.525 are also considered. All other parameters in the two cases are the same as those of the case with the bump in Fig. 22. The comparison of the responses of the Wigley Hull for all the cases is shown in Figure 24. The difference between these results exists in the phases and the amplitudes. The shift in the phase relative to the curve for the flat seabed (z_{sb}=*0*) becomes larger with the increase of z_{sb},(Fig. 24 a-f). The change in the amplitude is different for different motion components. The amplitudes of the surge, heave and pitch (Fig. 24 a-c) seem not to change dramatically but those of sway, roll and yaw (Fig. 24 d-f) increase significantly as the increase of z_{sb}. That is perhaps because these three components are mainly caused by the appearance of the bump; without it, they are very small as shown in the figure for the case with z_{sb}=0. In addition, it is interesting to note that for z_{sb}=0.7, the magnitude of sway is larger than that of heave and the magnitude of roll is similar to that of pitch, indicating how important the effect of a high bump is on the magnitudes.

[Figure24a]

Fig. 24 (a) surge

[Figure24b]

Fig. 24 (b) heave

[Figure24c]

Fig. 24 (c) pitch

[Figure24d]

Fig. 24 (d) sway

[Figure24e]

Fig. 24 (e) roll

[Figure24f]

Fig. 24 (f) yaw

Fig. 24 Responses of the Wigley Hull in cases with different heights of the bump ($r_x = 7$, $r_y = 3$, $\alpha_{sb} = 1$, $\omega = 1.7691$, a=0.03, d_b=1)

As shown in Fig. 22, the bump may result in very different forms of wave: from long crested to short crested in some area, and different amplitudes at different positions. That means that a floating body may have different responses if it is put into different positions. To partly show this, more cases are presented here, in which the distance (d_b) of the floating body centre from the wall at y=3 varies in the range of (0.5, 1, 2, 3) with other parameters remaining the same as for Fig. 24 with the bump. The second case in this series is actually the one discussed in that figure. To illustrate the effect of the position variation, the sway, roll and yaw motions of the Wigley hull located at different positions are depicted in Fig. 25. As can be seen, the maximum magnitudes of all these components are increased when the floating body become closer to the wall from d_b=3 to d_b=1. However, when the position changes from d_b=1 to d_b=0.5, the maximum

amplitudes of sway and roll become smaller while that of yaw remains similar. Thus, the results confirm that the responses of the floating body are sensitive to where it is located when the seabed is not flat.

[Figure25]

Fig. 25 Response of the Wigley Hull located at different positions
(z_{sb} =0.7, $r_x = 7, r_y = 3$, $\alpha_{sb} = 1$, $\omega = 1.7691$, a=0.03)

[Figure26]

Fig. 26 Snapshots of the part of the free surface near two identical Wigley Hulls in waves
($\omega = 1.7691$, a=0.04; L=15, B=6; $\tau \approx 52.1$)

5.3. Two Wigley Hulls floating over a flat seabed

So far, all discussions have focused on the problems about a single body. In many applications, one may deal with situations where two vessels are close to each other. Configurations of the two vessels may

vary, such as both in a head sea, both in oblique waves or one in a head sea with the other in an oblique wave. No matter which configuration is used, the vessels in all the cases undergo 6-DoFs motions. Fully nonlinear analysis on this kind of problem is extremely challenging and has not yet been found so far in the public domain. In this subsection, the presentation is devoted to some cases of this kind analysed by the method described in previous sections.

[Figure27]

Fig. 27 Responses of two Wigley Hulls to waves (a=0.04, ω=1.7691, d_{sb}=0.6)

Fig. 26 shows an example of two identical Wigley Hulls in the waves generated by the wavemaker with $\omega = 1.7691$ and a=0.04, resulting in a wave steepness of about 0.075. In this case, each of the two Wigley Hulls is the same as that used in Fig. 22. The centres of the Wigley hulls are initially located at x=0, y=-0.3 (No. 1) and x=0, y=0.3 (No.2), respectively. The distance between the centres of these two hulls (d_{sb}) is 0.6 (3 times the width of the hull). They are all in head sea. Nevertheless, each of them will undergo motions of 6 DoFs with the sway, roll and yaw being solely caused by the interaction between the two hulls. The width of the tank is 6 and its length is 15. According to the numerical tests, the responses of the hulls calculated by using this tank have less than 0.1% difference with those from the case with the tank width of 8 when $\tau \le 60$. The time histories of sway, roll and yaw of these two hulls are shown in Fig. 27. As can be seen, although they are not very large in terms of the amplitude, the time histories clearly contain many

components of different frequencies. One may also see that the three motion components of one hull are anti-symmetrical with these of the other because the problem as a whole is symmetrical about the *oxz* plane. Based on this, it is possible to simulate the case using half of the domain and one of the two bodies by applying a symmetrical boundary condition at y=0. To show this, Fig. 28 gives the comparison of the sway force acting on the No. 1 Hull calculated by using the whole domain and the half-domain, respectively. The difference seems to be negligible. Therefore, the half-domain may be used for similar configurations to save CPU times.

[Figure28]

Fig. 28 Comparison of the sway force acting on the No.1 Hull calculated by using the whole domain and the half-domain with a symmetrical boundary (a=0.04, ω=1.7691, d_{sb}=0.6)

As illustrated in Fig. 28, the sway force includes higher frequency (about twice the wave frequency) components. It must result from the nonlinear effects. To further show this, the hydrodynamic forces/moments due to waves generated by different amplitudes (a=0.004 and a=0.04) of the wavemaker are compared in Fig. 29. One may observe that the higher frequency components clearly exist in the forces or moments for the case with the larger amplitude while they are not evident in the case with the smaller amplitude. For the sway force (Fig. 29a), the apparent period between two successive zero up-crossing points is about half of the wave period. In addition, the maximum value of sway force or roll moment is larger than that predicted by using the smaller amplitude (a=0.004). This fact calls for the necessity of using the nonlinear theory to numerically predict the responses of two Wigley Hulls in order to ensure the safety.

[Figure29a]

Fig. 29 (a) sway force

[Figure29b]

Fig. 29 (b) roll moment

[Figure29c]

Fig. 29 (c) yaw moment

Fig. 29 Hydrodynamic force/moment acting on Wigley Hull No.1 subjected to waves with different amplitudes

[Figure30]

Fig. 30 Snapshots of the part of free surface and the position of Wigley hulls ($\omega = 1.7691$, a=0.03; L=15, B=6; (a): $\tau \approx 58.69$, L_b=1.0,B_b=0.2 and D_r=0.15, $\theta_i = 30^o$; (b) $\tau \approx 53.7$, L_b=2.5,B_b=0.4 and D_r=0.3, $\theta_i = 0$ for No.1 and L_b=1.0,B_b=0.2 and D_r=0.15, $\theta_i = 20^o$ for No.2)

Although the case shown in Fig. 26 may be modelled using a half-domain for a single body, one may have to perform the analysis in the whole domain for two bodies in many other unsymmetrical applications. For example, two bodies are in oblique waves or one body is larger than the other. We could not present all such results in one paper but some illustrations will be given in the rest of this subsection with more details discussed elsewhere. For this purpose, some snapshots are shown in Fig. 30. Fig. 30 (a) depicts the case for the two identical Wigley Hulls in the oblique wave with the incident angle (θ_i) of 30°. The sizes of the hull are assigned as L_b=1.0, B_b=0.2 and D_r=0.15 and the distance between them is d_{sb}=1.0. Fig. 30(b) shows the case for two hulls of different sizes that are L_b=2.5 B_b=0.4 and D_r=0.3 for the larger one, and that are L_b=1.0 B_b=0.2 and D_r=0.15 for the smaller one. The incident angle of the wave to the larger one is zero

while it is 20° for the smaller one. The distance between their centres is d_{sb} =1.5. In both figures, the incident waves are generated by a piston wavemaker with $\omega = 1.7691$ and a=0.03 in a tank with length of 15 and width of 6.

6. Discussions on the mesh quality and the efficiency of the QALE-FEM for 3D floating bodies

One of the distinctive features of the QALE-FEM is that the unstructured mesh is moved at every time step to conform to the motions of boundaries. It is understood that the mesh quality is continuously varying during simulation. Therefore, how the mesh quality varies needs to be examined. For 2D cases with or without floating bodies, the mesh quality has been investigated qualitatively and illustrated by plotting the mesh in [18], [19] and [47]. In 3D cases, it is difficult to illustrate the internal elements by just plotting the mesh; and the quantitative analysis, in place of the qualitative analysis, is more convincing. In this paper, two different methods are used to look at the mesh quality quantitatively: quality distribution and aggregate quality. The quality distribution denotes how the quality index (q_e) of elements calculated by Eq. (32) is distributed at a certain instant. The aggregate quality of the mesh ([60]) is estimated by

$$Q_s(t) = M / \sum_{e=1}^{M} \frac{1}{q_e}, \tag{53}$$

where M is the number of elements in the whole fluid domain. The aggregate quality $Q_s(t)$ has only one value at one time step. The larger the value, the better the mesh quality is. It is obvious that the quality distribution is suitable to show the mesh quality at a time step while the aggregate quality is convenient for illustrating how the mesh quality varies during the whole period of simulation.

For all the cases presented in this paper, the mesh quality has been examined by using the two methods to ensure that the mesh quality is satisfactory during the simulation. One typical example is presented here; that is the case shown in Fig. 28. In this case, the two Wigley Hulls are involved but only half the domain with a single body is considered due to symmetry. The half fluid domain is discretised into about 847,254 elements and 154,342 nodes. The aggregate quality of the mesh during the long-time calculation is shown in Fig. 31. One can see that the aggregate quality is about 0.64 initially and it always remains larger than 0.62, though it fluctuates in a small range. Fig. 32 depicts the quality distribution of all elements at two time steps apart from that at the initial step, where the horizontal axis denotes the ranges of quality index and the vertical axis gives the percentage of elements whose quality indexes fall in a range of quality index. For

instance, about 40% elements fall in the range 0.6-0.7. The aggregate quality at the two time steps (τ=30 and τ=60) almost reaches the minimum as could be seen from Fig. 31. Even at such instants, the quality distributions are almost the same as that of the initial step - about 80% of elements having the quality index larger than 0.5, as seen in Fig. 32. More importantly, very bad elements (quality indexes less than 0.1) never appear during the calculation. All these facts imply that the quality of the mesh is retained throughout simulation.

[Figure31]

Fig. 31 Change of aggregate quality with time
($\omega = 1.7691$, a=0.04, two identical Wigley Hulls with L_b=1.0, B_b=0.2, D_r=0.15 and d_{sb}=0.6)

To give some information about how efficient the QALE-FEM is, it is noted that all the cases presented in the paper can be run on normal PCs. More specifically, the above case (related to Figs. 31 and 32) is calculated on a PC with a Pentium IV 2.53GHz processor and 1G RAM. The average CPU time spent on every time step is about 25s in a simulation of 2000 time steps. It takes about 13.3 hours to achieve results of 15 wave periods. Even for the cases shown in Figs. 30 where the whole domain must be used, similar results can be achieved in just over one day. These demonstrate that the numeral analysis on the complicated problems about the fully-coupling and fully-nonlinear interaction between floating bodies and waves can be performed on a normal PC within an acceptable time. Such efficiency has not been demonstrated by other numerical methods based on the same nonlinear theory in literature.

[Figure32]

Fig. 32 Quality distribution at three time steps
($\omega = 1.7691$, a=0.04, two identical Wigley Hulls with L_b=1.0, B_b=0.2, D_r=0.15 and d_{sb}=0.6)

7. Conclusion

In this paper, the QALE-FEM has been further developed to model problems about fully-nonlinear and

fully-coupling interaction between 3D floating bodies and waves. In this method, the boundary value problems for the velocity potential and its time derivatives are solved by using a finite element method in a time marching procedure. Compared with the conventional finite element method for water wave problems, the QALE-FEM contains three distinctive techniques: 1) mesh moving using a robust spring analogy method specially developed for problems associated with the oscillating free surface and floating bodies, 2) velocity calculation on the free surface and body surfaces and 3) the iterative procedure for dealing with the full coupling between bodies and waves.

The main technical developments in this paper, as discussed in §3, are the techniques required for dealing with 3D nonlinear wave-body interactions. These include the technique for moving mesh near and on body surfaces, the scheme for calculating fluid velocity on body surfaces and a more efficient iterative procedure called ISITIMFB-M for tackling the full coupling between the motions of waves and bodies. The main application developments, as discussed in §5, lie in fully-nonlinear simulation of various cases associated with free responses of one or two 3D floating bodies to excitation of steep waves over a flat or complex seabed. These include a single body located over a flat bed, a single body floating near a big bump, two identical bodies in a head sea, two identical bodies in an oblique wave and two different bodies having different incident angles with respect to the incoming wave. These results reveal some interesting points. For example, the transient behaviour may be considerably affected by the natural frequencies and incident angles; the waves in the case for a body floating near a large bump on the seabed could become short-crested even the incoming wave is long-crested; and the interaction between multiple vessels should be carefully investigated by using fully nonlinear methods. Most of the results are first time published to the authors' best knowledge.

The method has been validated by comparing its numerical predictions with experimental data for two cases: a moored SPAR platform and a barge-type floating body. Good agreement has been achieved in all the comparisons. Although more validations may be done in future, the comparisons in this paper shed significant light on the accuracy of the method. The quality of mesh is examined, which shows that the good quality of mesh is retained during a long-period simulation. Assessments are also made on the efficiency of the method, which demonstrate that some useful results about the complicated cases could be obtained by using a normal PC within an acceptable time, such as 13 hours or one day. Such efficiency has never been achieved by using other numerical methods for fully nonlinear wave-body interaction problems as far as we

known.

9. Acknowledgement

This work is sponsored partially by Leverhulme Trust, UK (F/00353/G) and by EPSRC, UK (GR/R78701), for which the authors are most grateful.

10. Reference

1. Beck RF, Reed AM. Modern seakeeping computations for ships. in *Proceedings of 23rd ONR Symposium on Naval Hydrodynamics,* Val de Reuil, France 2000; 1-45.
2. Eatock Taylor R. On Modelling the Diffraction of Water Waves. *Ship Technology Research* 2007; 54:54-80.
3. Liu Y, Xue M, Yue DKP. Computations of fully nonlinear three-dimensional wave–wave and wave body interactions. Part 2. Nonlinear waves and forces on a body. *Journal of Fluid Mechanics* 2001; 438: 41-66.
4. Clauss GF, Steinhagen U. Numerical simulation of nonlinear transient waves and its validation by laboratory data. in *Proceedings of 9th International Offshore and Polar Engineering Conference (ISOPE1999)*, Brest, France, 1999; 368-375.
5. Lachaume C, Biausser B, Grilli ST, Fraunie P, Guignard S. Modeling of Breaking and Post-breaking Waves on Slopes by Coupling of BEM and VOF Methods. in *Proceedings of 13th International Offshore and Polar Engineering Conference (ISOPE2003)*, Honolulu, HI, United States, 2003; 1698-1704.
6. Yang C, Lohner R, Lu H. An unstructured-grid based volume-of-fluid method for extreme wave and freely-floating structure interactions. *Journal of Hydrodynamics, Ser. B* 2006; 18: 415-422.
7. Idelsohn SR, Oñate E, Del Pin F, Calvo N. Fluid–structure interaction using the particle finite element method. *Computer Methods in Applied Mechanics and Engineering* 2006; 195: 2100-2123.
8. Turnbull MS, Borthwick AGL, Eatock Taylor R. Wave–structure interaction using coupled structured–unstructured finite element meshes. *Applied Ocean Research* 2003; 25: 63-77.
9. Heinze C. Nonlinear hydrodynamic effects on fixed and oscillating structures in waves. *PhD Thesis*, Department of Engineering Science, Oxford University, 2003.
10. Wang CZ, Wu GX. An unstructured-mesh-based finite element simulations with non-wall-sided bodies. *Journal of fluids and structures* 2006; 22: 441-461.
11. Wu GX, Eatock Taylor R. Transient motion of floating body in steep water waves. In: *Proceedings of the 11th International Workshop on Water Waves and Floating Bodies, Hamburg* 1996.
12. Dalen EFG. Numerical and theoretical studies on water waves and floating bodies. *PhD thesis*, University of Twente, Enschede, 1993.
13. Cao Y, Beck RF, Schultz WW. Nonlinear Computation of Wave Loads and Motions of Floating bodies in Incident Waves. in: *Proceedings of 9th International Workshop on Water Waves and Floating Bodies*, Kuju, Oita, Japan, 1994; 33-37.
14. Contento G. Numerical wave tank computations of nonlinear motions of two-dimensional arbitrarily shaped free floating bodies. *Ocean Engineering* 2000; 27: 531-556.
15. Kashiwagi M. Nonlinear simulations of wave-induced motions of a floating body by means of the mixed

Eulerian-Lagrangian method. *Proceedings of the Institution of Mechanical Engineers. Part C, Journal of mechanical engineering science* 2000; 214: 841-855.

16. Wu GX, Eatock Taylor R. The coupled finite element and boundary element analysis of nonlinear interactions between waves and bodies. *Ocean Engineering* 2003; 30:387-400.
17. Koo W, Kim M. Freely floating body simulation by a 2D fully nonlinear numerical wave tank. *Ocean Engineering* 2004; 31: 2011-2046.
18. Yan S, Ma QW. Numerical simulation of fully nonlinear interaction between steep waves and 2D floating bodies using the QALE-FEM method. *Journal of Computational Physics* 2007; 221: 666-692.
19. Yan S, Ma QW. Effects of an arbitrary sea bed on responses of moored floating structures to steep waves. In *Proceeding of 17th International Offshore and Polar Engineering* Conference (ISOPE2007), Lisbon, Portugal, 2007; 2192-2199.
20. Ferrant P. Fully nonlinear interactions of long-crested wave packets with a three-dimensional body. In *Proceedings of the 22nd ONR Symposium on Naval Hydrodynamics*, Washington DC, 1998; 403-15.
21. Ma QW. Numerical simulation of nonlinear interaction between structures and steep waves. *PhD Thesis*, Department of Mechanical Engineering, University College London, UK,1998.
22. Büchmann B, Ferrant P, Skourup J. Run-up on a body in waves and current. Fully nonlinear and finite-order calculations. *Applied Ocean Research* 2000; 22: 349-360.
23. Ma QW, Wu GX, Eatock Taylor R. Finite element simulation of fully non-linear interaction between vertical cylinders and steep waves. Part 1: Methodology and numerical procedure. *International Journal for Numerical Methods in Fluids* 2001; 36(3): 265-285.
24. Ma QW, Wu GX, Eatock Taylor R. Finite element simulation of fully non-linear interaction between vertical cylinders and steep waves. Part 2: Numerical results and validation, *International Journal for Numerical Methods in Fluids* 2001; 36(3) 287-308.
25. Celebi MS. Nonlinear Transient Wave-body Interactions in Steady Uniform Currents, Computer Methods in Applied Mechanics and Engineering 2001; 190: 5149-5172.
26. Corte C, Grilli ST. Numerical Modeling of Extreme Wave Slamming on Cylindrical Offshore Support Structures. In *Proceedings of 16th Offshore and Polar Engineering. Conference (ISOPE06)*, San Francisco, California ,2006; 394-401.
27. Wang CZ, Wu GX, Drake KR. Interactions between nonlinear water waves and non-wall-sided 3D structures. *Ocean Engineering* 2007; 34: 1182-1196.
28. Bai W, Eatock Taylor R. Numerical simulation of fully nonlinear regular and focused wave diffraction around a vertical cylinder using domain decomposition. *Applied Ocean Research* 2007; 29: 55-71.
29. Scorpio S, Beck RF, Korsrneyer T. Nonlinear water waves computations using a multipole accelerated desingularized method. In *Proceedings of 21st Symposium on Naval Hydrodynamics*, Norwegian Institute of Technology, Trondheim, Norway, 1996; 64-75.
30. Celebi MS, Kim MH, Beck RF. Fully nonlinear 3D numerical wave tank simulation. *Journal of Ship Research* 1998; 42: 33–45.
31. Kim MH, Celebi MS, Kim DJ. Fully nonlinear interactions of waves with a three-dimensional body in uniform currents. *Applied Ocean Research* 1998; 20: 309–321.
32. Bai W, Eatock Taylor R. Higher-order boundary element simulation of fully nonlinear wave radiation by oscillating vertical cylinders. *Applied Ocean Research* 2006; 28: 247-265.

33. Tanizawa K, Minami M. Development of a 3D-NWT for simulation of running ship motions in waves. In *International Workshop on Water Waves and Floating Bodies*, Hiroshima, Japan, 2001.
34. Yan S., Ma QW. QALE-FEM for modelling 3D overturning waves, submitted for publication but some results are given at www.staff.city.ac.uk/q.ma, 2008.
35. Longuet-Higgins MS, Cokelet ED. The deformation of steep waves on water: I. a numerical method of computation. *Proceedings of the Royal Society of London. Series A* 1976; 350: 1–26.
36. Vinje T, Brevig P. Nonlinear ship motion. In *Proceeding of 3rd International Conference on Numerical Ship Hydrodynamics*, Paris, France, 1981; 257–268.
37. Lin WM, Newman JN, Yue DKP. Nonlinear forced motion of floating bodies. In *Proceedings of 15th Symposium on Naval Hydrology*, Hamburg, Germany, 1984; 33–49.
38. Wang P, Yao Y, Tulin M. An efficient numerical tank for nonlinear water waves, based on the multi-subdomain approach with BEM. *International Journal for Numerical Methods in Fluids* 1995; 20: 1315-1336.
39. Grilli ST, Guyenne P, Dias F. A fully nonlinear model for three-dimensional overturning waves over arbitrary bottom. *International Journal for Numerical Methods in Fluids* 2001; 35: 829-867.
40. Kashiwagi M. Full-nonlinear simulations of hydrodynamic forces on a heaving two-dimensional body. *Journal of the Society of Naval Architects of Japan* 1996; 180: 373–381.
41. Cao Y, Schultz WW, Beck RF. Three-dimensional desingularised boundary integral method for potential problems. *International Journal for Numerical Methods in Fluids* 1991; 12: 785-803.
42. Fochesato C, Dias F. A fast method for nonlinear three-dimensional free-surface waves. *Proceedings of the Royal Society of London. Series A* 2006; 462: 2715-2735.
43. Wu GX, Eatock Taylor R. Finite element analysis of two dimensional non-linear transient water waves. *Applied Ocean Research* 1994; 16: 363–372.
44. Wu GX, Eatock Taylor R. Time stepping solution of the two dimensional non-linear wave radiation problem. *Ocean Engineering* 1995; 22: 785–798.
45. Westhuis JH, Andonowati AJ. Applying the finite element method in numerically solving the two dimensional free-surface water wave equations. In *13th International Workshop on Water Waves and Floating Bodies*, Alphenaan den Rijn, The Netherlands, Hermans AJ (ed.), 1998; pp. 171–174.
46. Wu GX, Hu ZZ. Simulation of nonlinear interactions between waves and floating bodies through a finite-element-based numerical tank. *Proceedings of the Royal Society of London. Series A* 2004; 460: 3037-3058.
47. Ma QW, Yan S. Quasi ALE finite element method for nonlinear water waves. *Journal of Computational Physics* 2006; 212: 52-72.
48. Tanizawa K. A nonlinear simulation method of 3-D body motions in waves: formulation with the acceleration potential. In *10th International Workshop on Water Waves and Floating Bodies,* Oxford, UK, 1995.
49. Tanizawa K. A nonlinear simulation method of 3-D body motions in waves (1st Report): Formulation of the method with acceleration potential. *Journal of the Society of Naval Architects of Japan* 1995; 178: 179-191.
50. Tanizawa K, Minami M. On the accuracy of NWT for radiation and diffraction problem. In *Proceeding of 6th Symposium on Nonlinear and Free-Surface Flow*, 1998.
51. Tanizawa K, Minami M, Naito S. Estimation of wave drift force by numerical wave tank. In *Proceeding*

of 9th International Offshore and Polar Engineering Conference (ISOPE1999), Brest, 1999; 3: 323-330.

52. Kashiwagi M, Momoda T, Inada M. A time-domain nonlinear simulation method for wave-induced motions of a floating body. *Journal of the Society of Naval Architects of Japan* 1998; 84: 143–152.
53. Tanizawa K. The state of the art on numerical wave tank. In *Proceeding of 4th Osaka colloquium on seakeeping performance of ships*, Osaka, Japan, 2000; 95-114.
54. Ma QW, Patel MH. On the nonlinear forces acting on a floating spar platform in ocean waves. *Applied Ocean Research* 2001; 23: 29-40.
55. Yan S. Numerical simulation of nonlinear response of moored floating structures to steep waves, *PhD Thesis*, School of Engineering and Mathematical Sciences, City University, London, UK, 2006.
56. Frey PJ, Borouchaki H, George P. 3D Delaunay mesh generation coupled with an advancing-front approach. *Computer Methods in Applied Mechanics and Engineering* 1998; 157: 115-131.
57. Batina JT. Unsteady Euler Airfoil Solutions Using Unstructured Dynamic Meshes, *AIAA Paper 89-0115, 27th AIAA Aerospace Sciences Meeting*, Reno, NV, 1989.
58. Farhat C, Degand C, Koobus BM, Lesoinne M. A three-dimensional torsional spring analogy method for unstructured dynamic meshes. *Computers and Structures* 2002; 80: 305-316.
59. Bottasso CL, Detomi D, Serra R. The ball-vertex method: a new simple spring analogy method for unstructured dynamic meshes. *Computer methods in applied mechanics and engineering* 2005; 194: 4244-4264.
60. Lewis RW, Zheng Y, Gethin DT. Three-dimensional unstructured mesh generation: Part 3. Volume meshes. *Computer Methods in Applied Mechanics and Engineering* 1996; 134: 285-310.
61. Ma QW. Meshless local Petrov-Galerkin method for two-dimensional nonlinear water wave problems. *Journal of Computational Physics* 2005; 205: 611-625.
62. Grue CW, *Numerical Initial Value Problems in Ordinary Differential Equations.* Prentice-Hall, Inc. Englewood Cliffs, New Jersey, 1971; 102-115.
63. Weggel DC, Roesset JM, Davies RL, Steen A, Frimm F. Neptune Project: Spar history and design considerations. In: *OTC 8382, Offshore Technology Conference,* Houston, TX, USA, 2, 1997; 237-251.
64. Shashikala AP, Sundaravadivelu R, Ganapathy C. Dynamics of a moored barge under regular and random waves. *Ocean Engineering* 1997; 24: 401-430.
65. Grilli ST, Horrillo J. Shoaling of periodic waves over barred-beaches in a fully nonlinear numerical wave tank. *International Journal of Offshore and Polar Engineering* 1999; 9: 257-263.

Table 1. Summary of problems about fully nonlinear interaction between waves and bodies

	Fixed body	Forced motion	Free response with 3 DoFs	Free responses with 6 DoFs (single body)	Free responses with 6 DoFs (multi-bodies)
2D bodies	Turnbull, et al [8]; Heinze [9]; Wang et al[10];	Wang et al[10]; Wu et al[11]	Dalen[12]; Cao et al [13]; Contento[14]; Kashiwagi[15]; Wu et al[16]; Koo et al[17]; Yan et al[18,19];	N/A	N/A
3D bodies	Ferrant [20]; Ma [21]; Büchmann et al [22]; Ma et al [23,24];Celebi [25];Corte et al[26]; Wang et al[27]; Bai et al [28];	Scorpio et al [29]; Celebi et al[30];Kim et al [31]; Wang et al[10]; Bai et al [32];	Tanizawa et al[33]	Very rare if not nothing	Very rare if not nothing

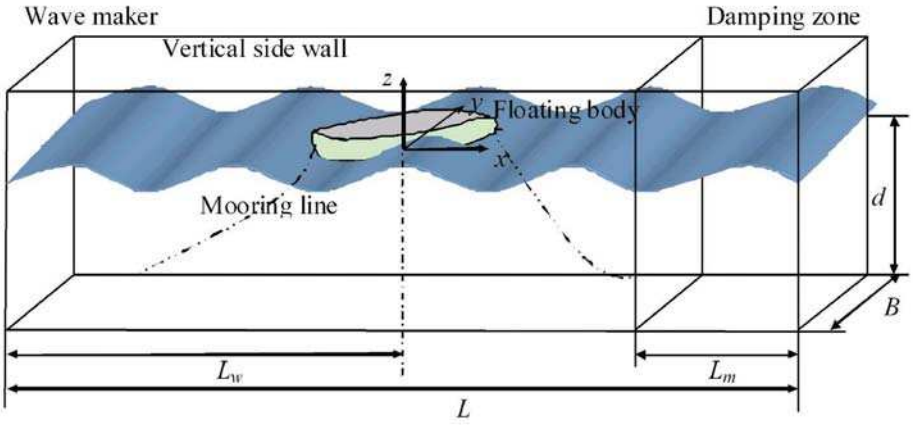

127x59mm (600 x 600 DPI)

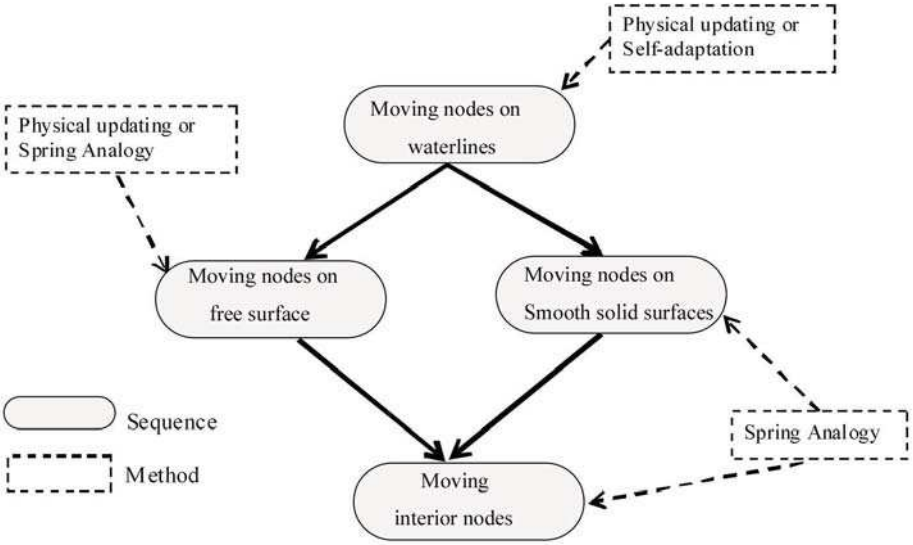

63x39mm (600 x 600 DPI)

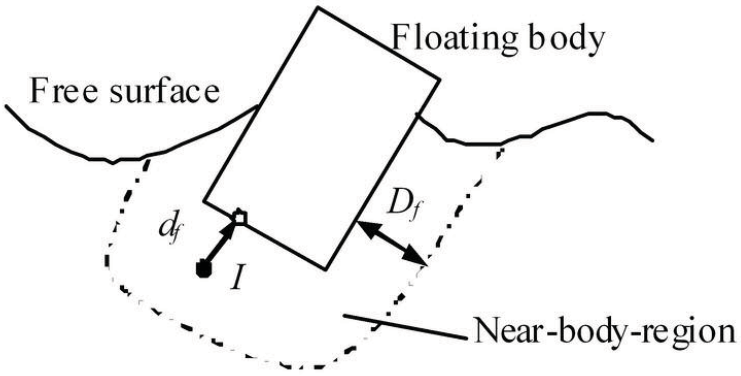

40x20mm (600 x 600 DPI)

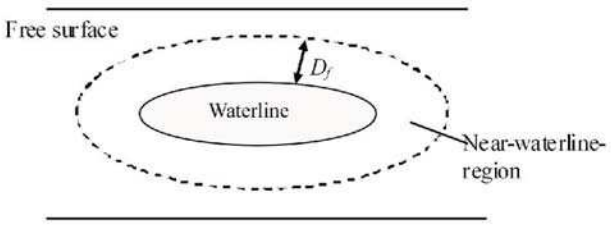

84x32mm (600 x 600 DPI)

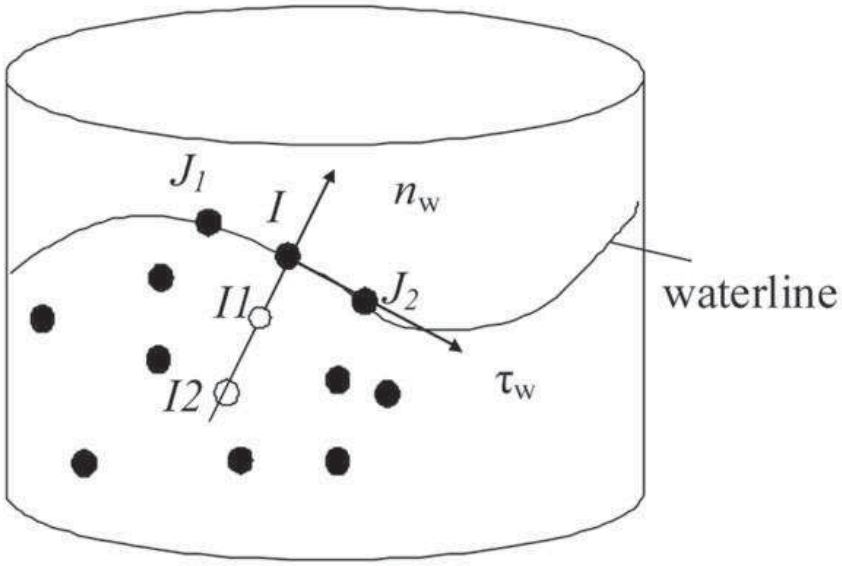

28x18mm (600 x 600 DPI)

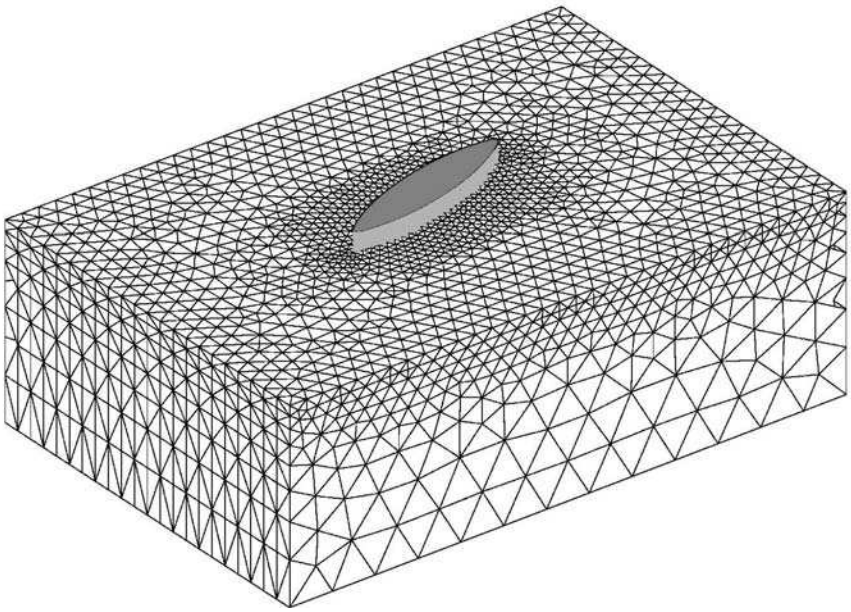

172x136mm (600 x 600 DPI)

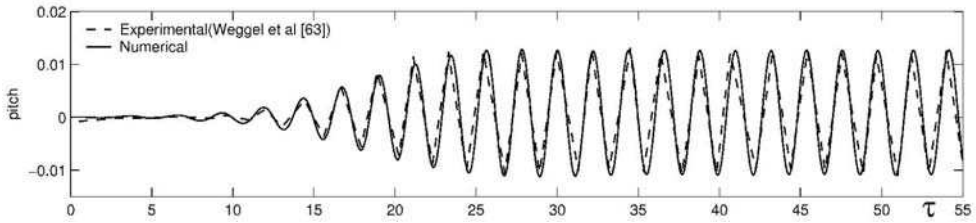

228x52mm (600 x 600 DPI)

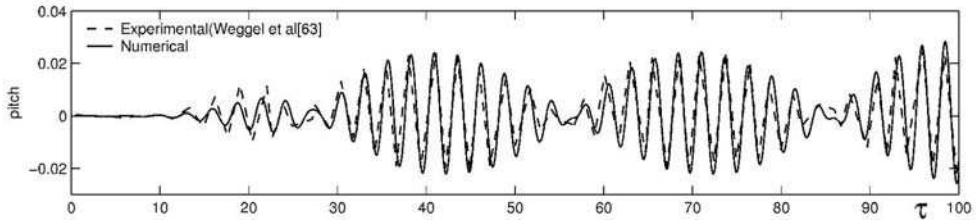

228x52mm (600 x 600 DPI)

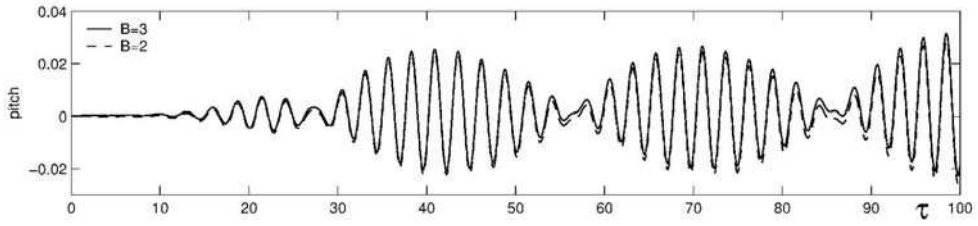

228x52mm (600 x 600 DPI)

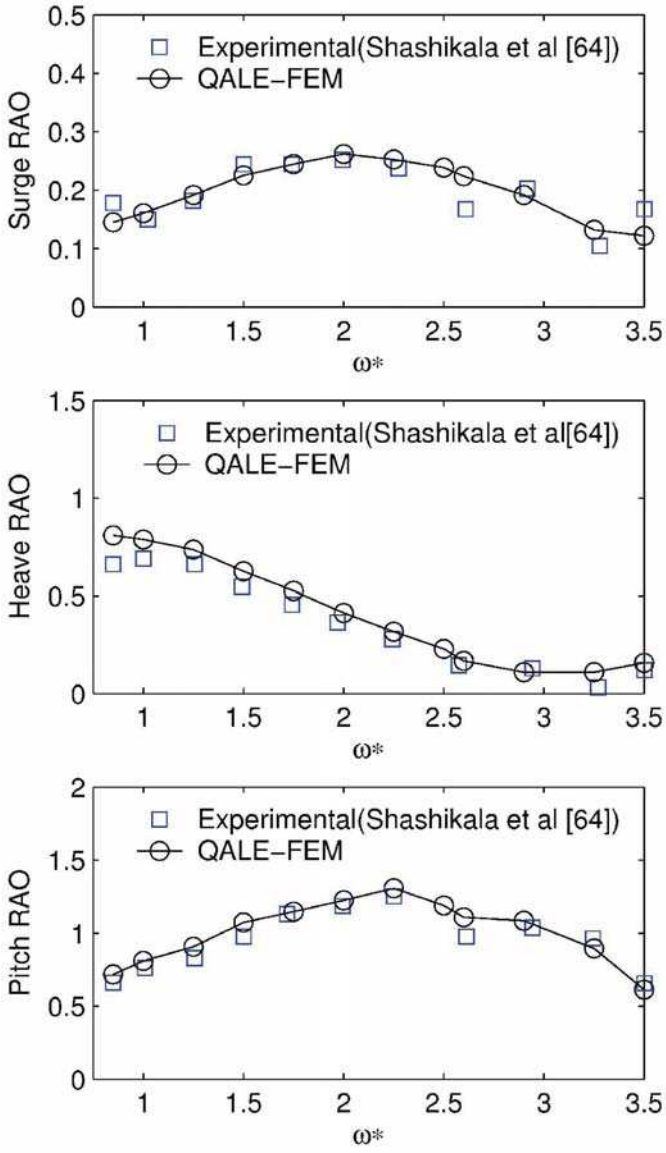

86x151mm (600 x 600 DPI)

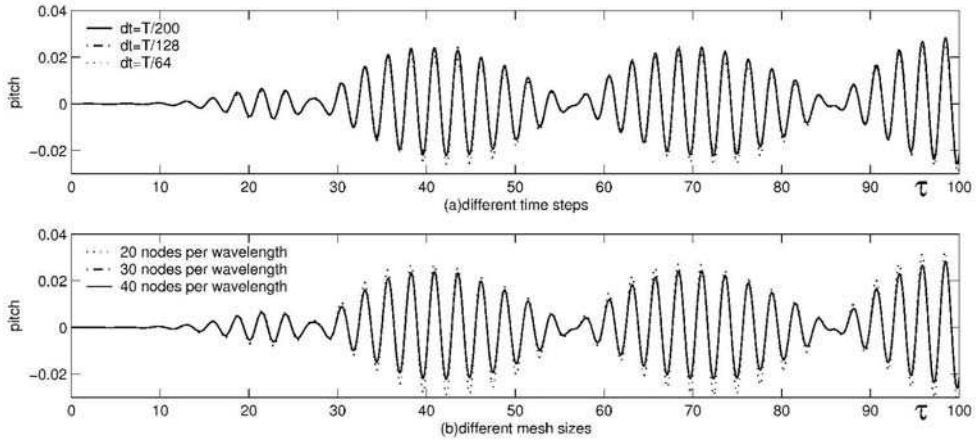

229x104mm (600 x 600 DPI)

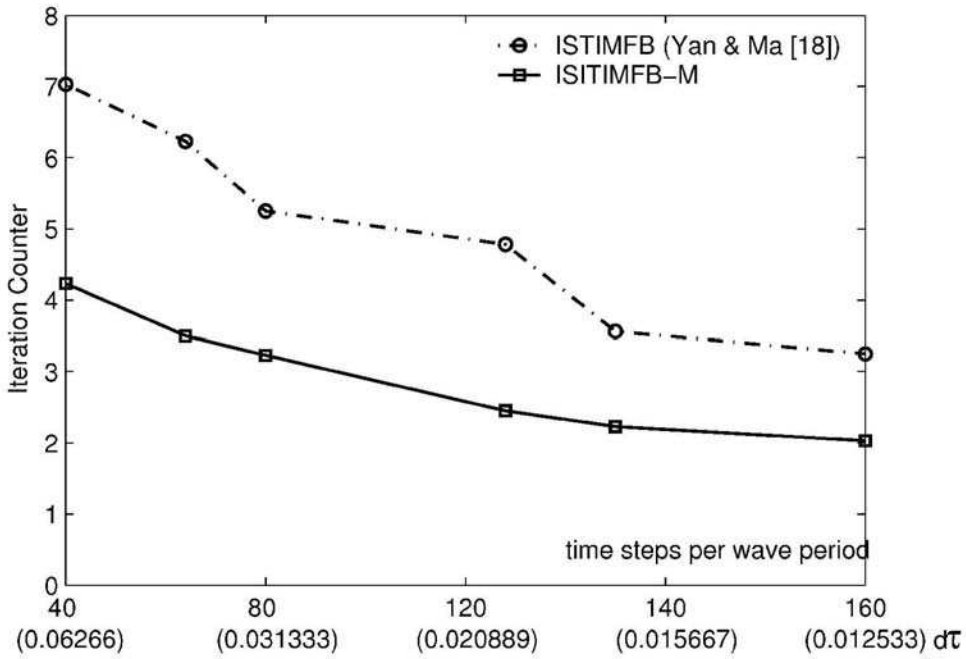

134x92mm (600 x 600 DPI)

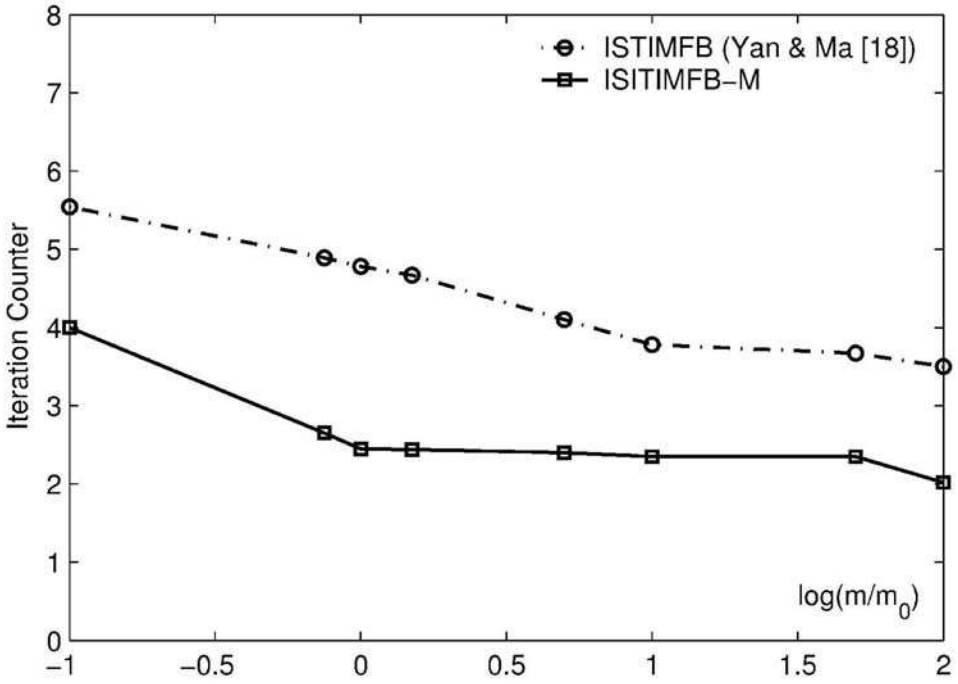

123x87mm (600 x 600 DPI)

228x53mm (600 x 600 DPI)

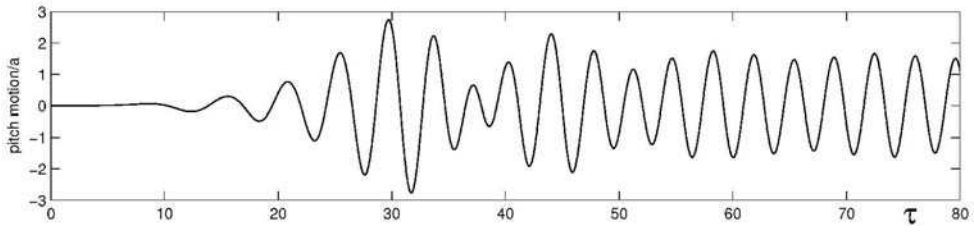

223x52mm (600 x 600 DPI)

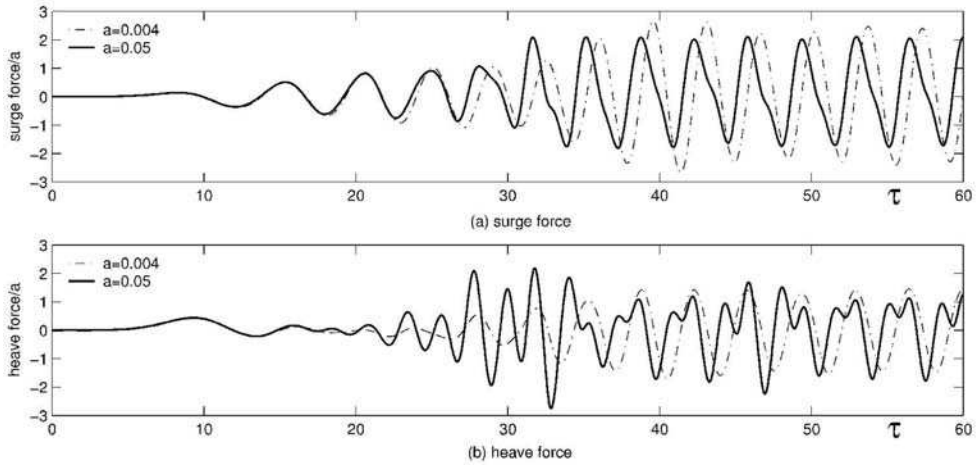

221x106mm (600 x 600 DPI)

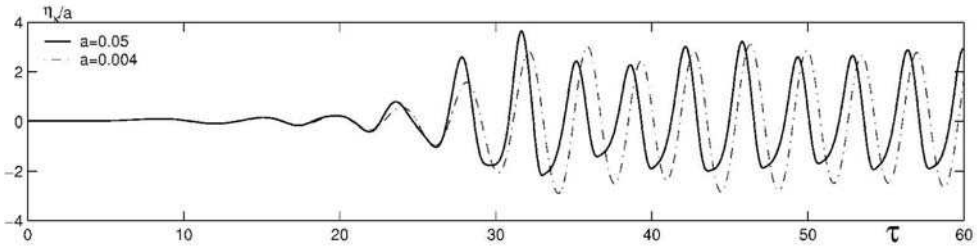

216x55mm (600 x 600 DPI)

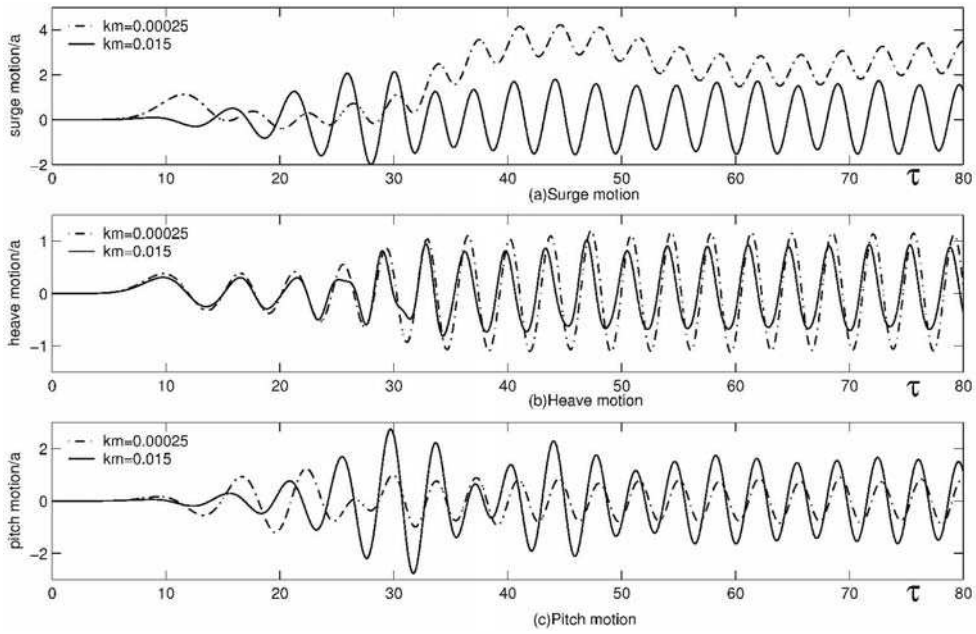

221x143mm (600 x 600 DPI)

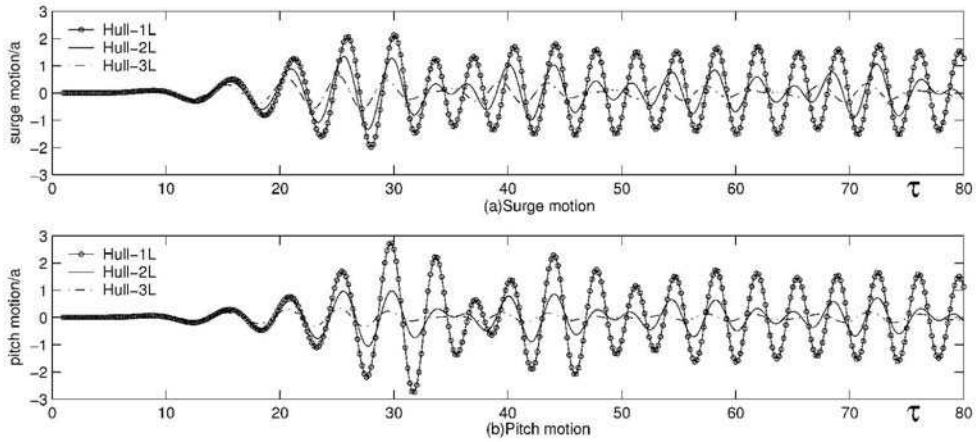

221x100mm (600 x 600 DPI)

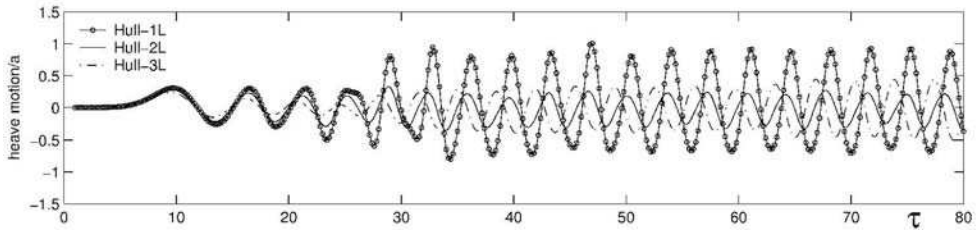

225x53mm (600 x 600 DPI)

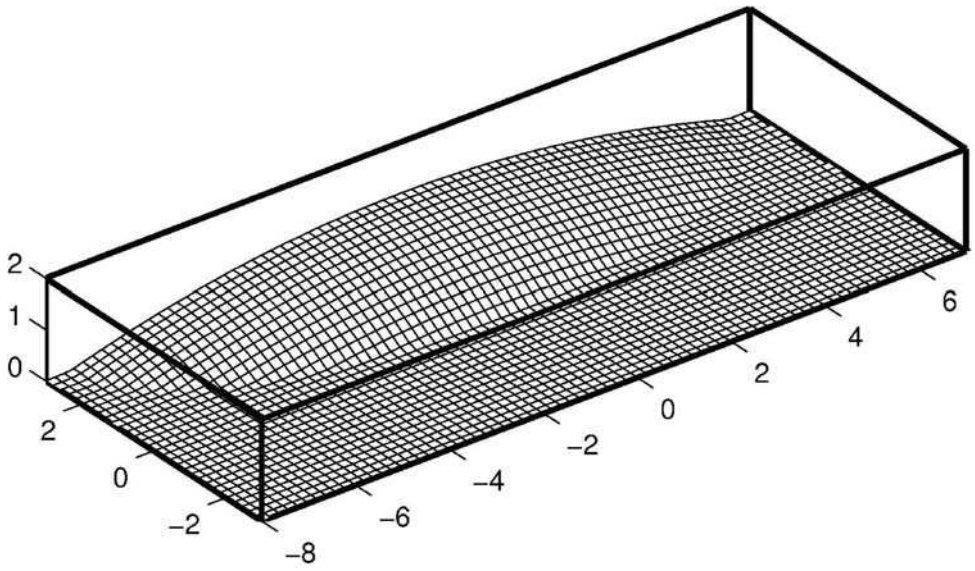

120x71mm (600 x 600 DPI)

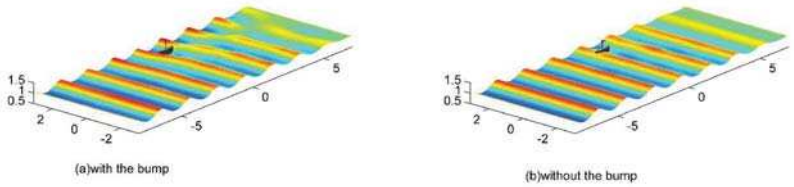

190x55mm (600 x 600 DPI)

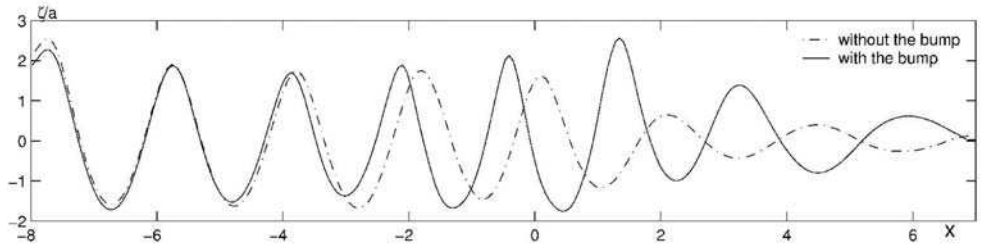

214x55mm (600 x 600 DPI)

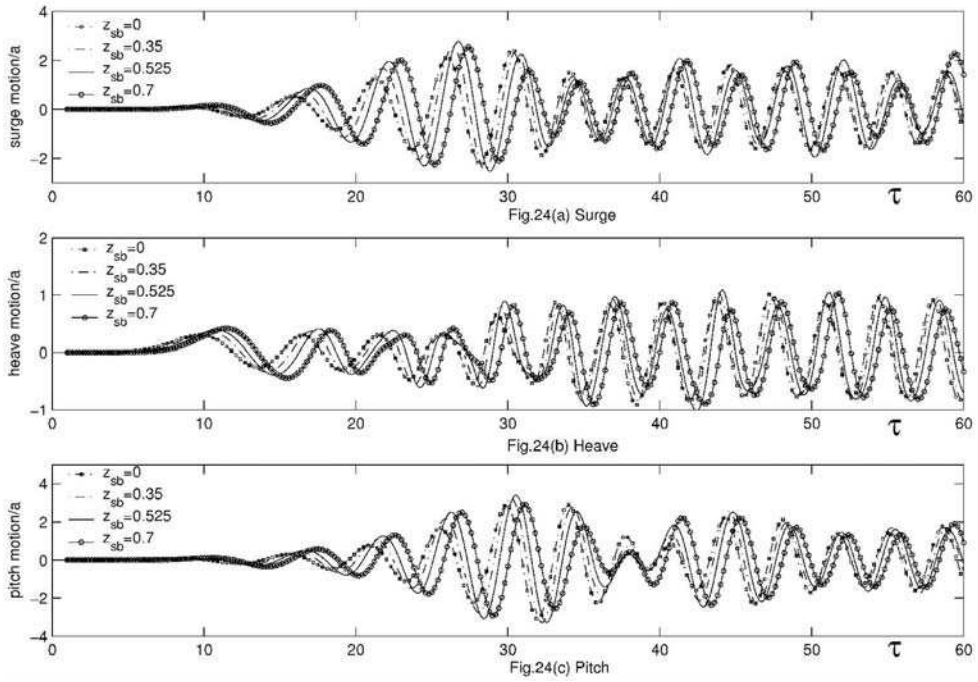

Fig.24(a) Surge

Fig.24(b) Heave

Fig.24(c) Pitch

221x155mm (600 x 600 DPI)

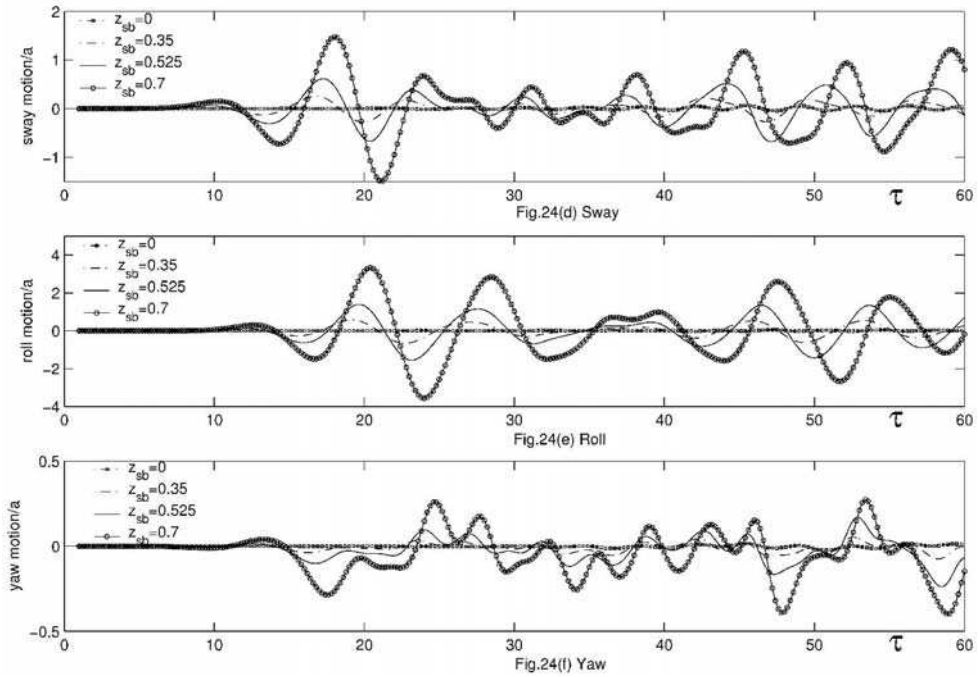

Fig.24(d) Sway

Fig.24(e) Roll

Fig.24(f) Yaw

224x155mm (600 x 600 DPI)

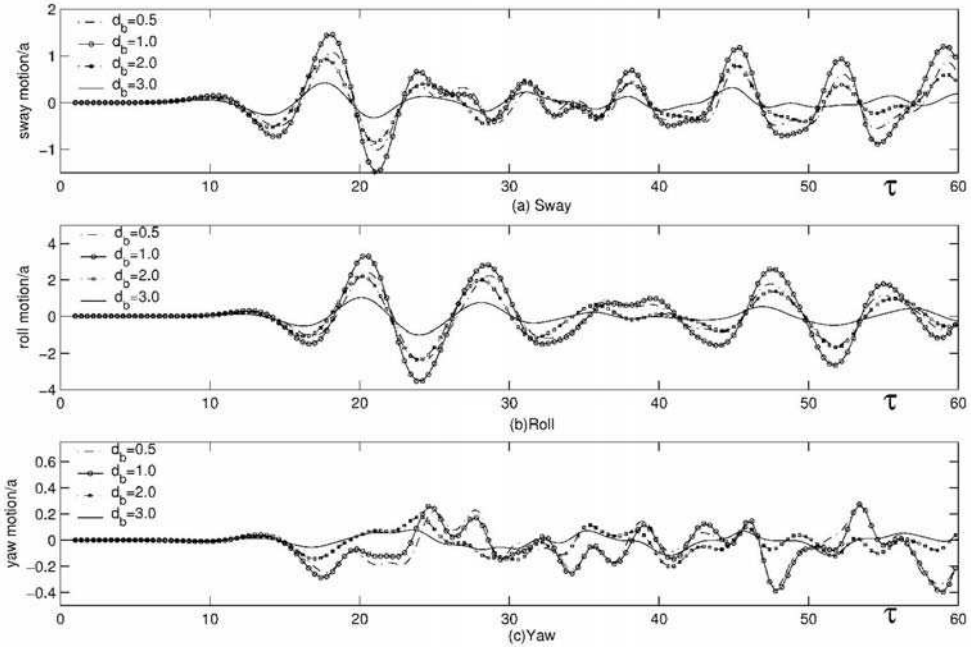

226x151mm (600 x 600 DPI)

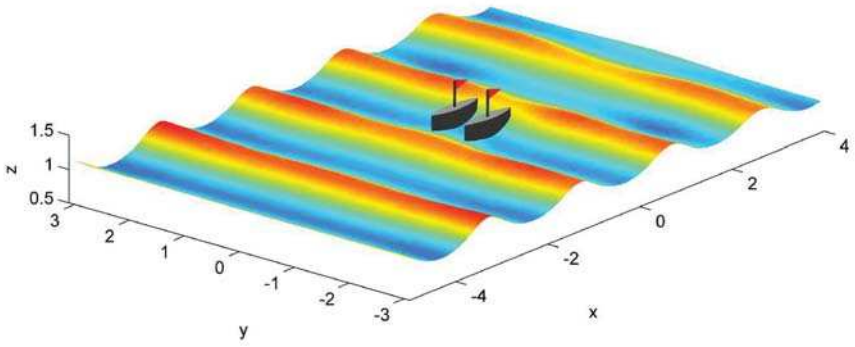

127x56mm (600 x 600 DPI)

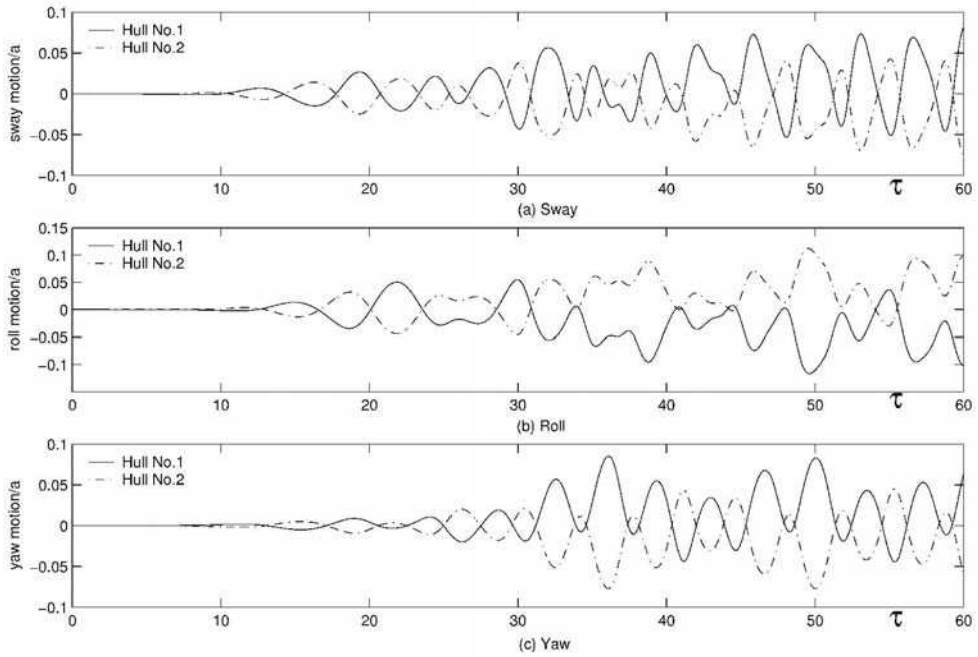

226x153mm (600 x 600 DPI)

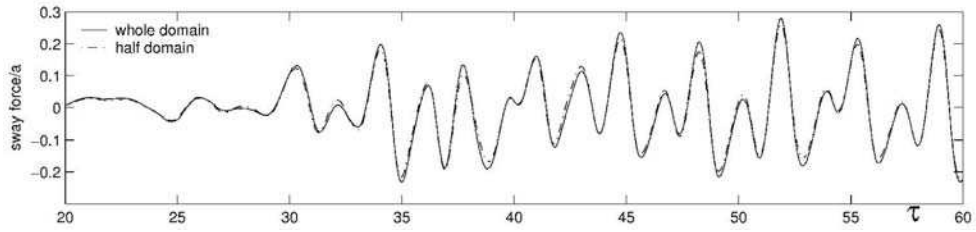

225x53mm (600 x 600 DPI)

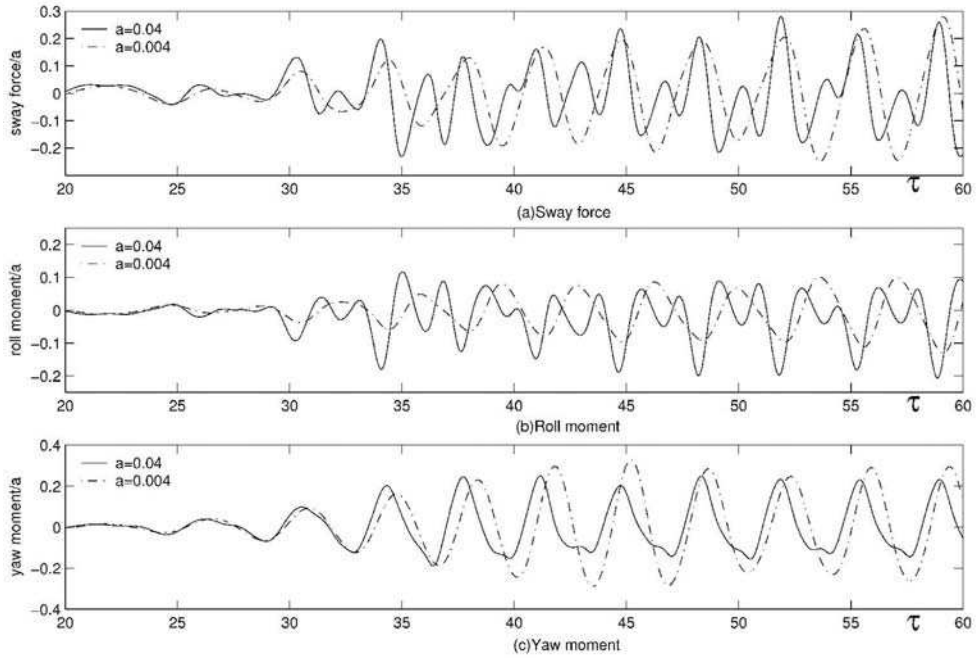

225x152mm (600 x 600 DPI)

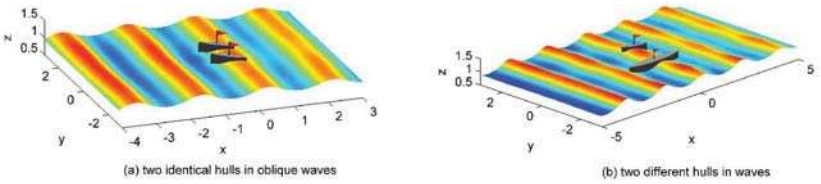

190x63mm (600 x 600 DPI)

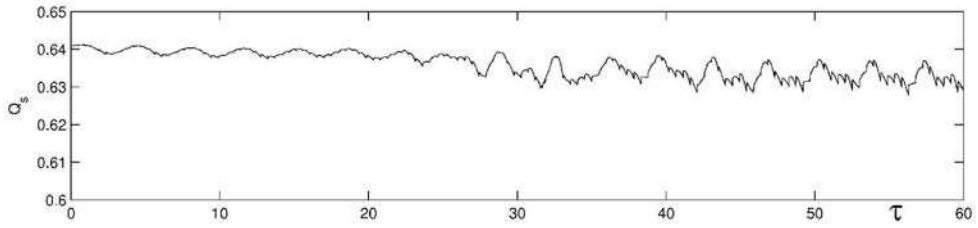

226x52mm (600 x 600 DPI)

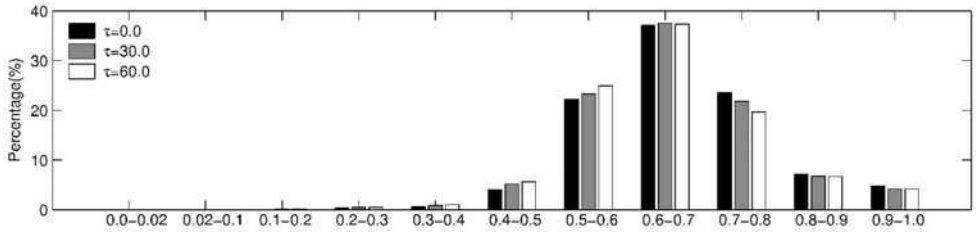

219x52mm (600 x 600 DPI)